A Section 508–conformant HTML version of this article is available at https://doi.org/10.1289/EHP7612.

The Kidney-Related Effects of Polystyrene Microplastics on Human Kidney Proximal Tubular Epithelial Cells HK-2 and Male C57BL/6 Mice

Yung-Li Wang,[1] Yu-Hsuan Lee,[2] Yung-Ho Hsu,[3,4,5] I-Jen Chiu,[1,5,6] Cathy Chia-Yu Huang,[7] Chih-Chia Huang,[8] Zi-Chun Chia,[8] Chung-Pei Lee,[9] Yuh-Feng Lin,[1,5,6,10*] and Hui-Wen Chiu[1,5,6,11]*

[1]Graduate Institute of Clinical Medicine, College of Medicine, Taipei Medical University, Taipei, Taiwan
[2]Department of Cosmeceutics, China Medical University, Taichung, Taiwan
[3]Division of Nephrology, Department of Internal Medicine, Hsin Kuo Min Hospital, Taipei Medical University, Taoyuan City, Taiwan
[4]Department of Internal Medicine, School of Medicine, College of Medicine, Taipei Medical University, Taipei, Taiwan
[5]Research Center of Urology and Kidney, Taipei Medical University, Taipei, Taiwan
[6]Division of Nephrology, Department of Internal Medicine, Shuang Ho Hospital, Taipei Medical University, New Taipei City, Taiwan
[7]Department of Life Sciences, National Central University, Taoyuan City, Taiwan
[8]Department of Photonics, Center of Applied Nanomedicine, National Cheng Kung University, Tainan, Taiwan
[9]School of Nursing, National Taipei University of Nursing and Health Sciences, Taipei, Taiwan
[10]Department of Internal Medicine, School of Medicine, National Defense Medical Center, Taipei, Taiwan
[11]Department of Medical Research, Shuang Ho Hospital, Taipei Medical University, New Taipei City, Taiwan

Background: Understanding the epidemic of chronic kidney disease of uncertain etiology may be critical for health policies and public health responses. Recent studies have shown that microplastics (MPs) contaminate our food chain and accumulate in the gut, liver, kidney, muscle, and so on. Humans manufacture many plastics-related products. Previous studies have indicated that particles of these products have several effects on the gut and liver. Polystyrene (PS)-MPs (PS-MPs) induce several responses, such as oxidative stress, and affect living organisms.

Objectives: The aim of this study was to investigate the effects of PS-MPs in kidney cells *in vitro* and *in vivo*.

Methods: PS-MPs were evaluated in human kidney proximal tubular epithelial cells (HK-2 cells) and male C57BL/6 mice. Mitochondrial reactive oxygen species (ROS), endoplasmic reticulum (ER) stress, inflammation, and autophagy were analyzed in kidney cells. *In vivo*, we evaluated biomarkers of kidney function, kidney ultrastructure, muscle mass, and grip strength, and urine protein levels, as well as the accumulation of PS-MPs in the kidney tissue.

Results: Uptake of PS-MPs at different concentrations by HK-2 cells resulted in higher levels of mitochondrial ROS and the mitochondrial protein Bad. Cells exposed to PS-MPs had higher ER stress and markers of inflammation. MitoTEMPO, which is a mitochondrial ROS antioxidant, mitigated the higher levels of mitochondrial ROS, Bad, ER stress, and specific autophagy-related proteins seen with PS-MP exposure. Furthermore, cells exposed to PS-MPs had higher protein levels of LC3 and Beclin 1. PS-MPs also had changes in phosphorylation of mitogen-activated protein kinase (MAPK) and protein kinase B (AKT)/mitogen-activated protein kinase (mTOR) signaling pathways. In an *in vivo* study, PS-MPs accumulated and the treated mice had more histopathological lesions in the kidneys and higher levels of ER stress, inflammatory markers, and autophagy-related proteins in the kidneys after PS-MPs treatment by oral gavage.

Conclusions: The results suggest that PS-MPs caused mitochondrial dysfunction, ER stress, inflammation, and autophagy in kidney cells and accumulated in HK-2 cells and in the kidneys of mice. These results suggest that long-term PS-MPs exposure may be a risk factor for kidney health. https://doi.org/10.1289/EHP7612

Introduction

Since 1950, plastic products have become inexpensive, durable, convenient, and useful in many aspects of human life, resulting in dramatic increases in the human use of these products (Geyer et al. 2017; Rhodes 2018). A previous study predicted that 33 billion tons of plastic will be produced in 2050 (Rochman et al. 2013). Plastic products are reusable but due to irresponsible waste recycling and a slow biodegradation rate, plastic has accumulated in the environment worldwide (Díaz-Torres et al. 2017; Jambeck et al. 2015; Lamb et al. 2018). As characterized by Lebreton et al. (2018), plastic waste accumulation in the Pacific Ocean had formed what is commonly called the Great Pacific Garbage Patch (Lebreton et al. 2018), from which plastic can be broken into small fragments via physicochemical decomposition to become microplastics (MPs) and nanoplastics (NPs) (Song et al. 2017; Yousif and Haddad 2013). In addition, the mixed synthetic fibers that compose the textiles we wear daily have also been shown to generate MPs or NPs during laundering (Carney Almroth et al. 2018), and the resulting particles have been found in the ocean (Remy et al. 2015). However, these MPs or NPs do not disappear. For example, plastic cigarette filters were shown to take 7.5–14 y to decompose (Joly and Coulis 2018). But some of the materials themselves may break into MPs or NPs (Song et al. 2017; Yousif and Haddad 2013). These particles cross the gut of living organisms and can enter the circulatory system via trophic transfer (Carbery et al. 2018). These MPs or NPs may accumulate in our food chain (Smith et al. 2018). MPs or NPs can also potentially accumulate in humans given that they had been shown to accumulate in the gut, liver, and kidneys in mice (Deng et al. 2017b; Yang et al. 2019) and in the muscle tissue of northern fulmars (Herzke et al. 2016) due to consumption of food items such as fish (Abbasi et al. 2018), seafood (Cho et al. 2019; Li et al. 2018; Van Cauwenberghe and Janssen 2014), milk (Kutralam-Muniasamy et al. 2020), beer (Kosuth et al. 2018; Liebezeit and Liebezeit 2014), sea salt (Iñiguez et al. 2017; Kosuth et al. 2018), sugar (Liebezeit and Liebezeit 2013), honey (Liebezeit and Liebezeit 2013), tea in plastic teabags (Hernandez et al. 2019), unfiltered water (Pivokonsky et al. 2018), tap water (Kosuth et al. 2018), and bottled water (Schymanski et al. 2018; Welle and Franz 2018).

Chronic kidney disease (CKD) results from many diverse disease pathways that change the structure and function of the kidneys

*These authors contributed equally to this work.

Address correspondence to Hui-Wen Chiu, Graduate Institute of Clinical Medicine, College of Medicine, Taipei Medical University, 250 Wuxing St., Taipei, Taiwan 110. Telephone: 886-2-22490088, ext. 8884. Email: leu3@tmu.edu.tw

Supplemental Material is available online (https://doi.org/10.1289/EHP7612).

The authors declare they have no actual or potential competing financial interests.

Received 4 June 2020; Revised 19 March 2021; Accepted 12 April 2021; Published 6 May 2021.

Note to readers with disabilities: *EHP* strives to ensure that all journal content is accessible to all readers. However, some figures and Supplemental Material published in *EHP* articles may not conform to 508 standards due to the complexity of the information being presented. If you need assistance accessing journal content, please contact ehponline@niehs.nih.gov. Our staff will work with you to assess and meet your accessibility needs within 3 working days.

and irreversibly damage kidney function (Webster et al. 2017). In a retrospective study, many hospitalized patients did not know that they suffered from CKD (Saunders et al. 2015). An epidemic of CKD of uncertain etiology (CKDu) is emerging worldwide (Gifford et al. 2017; Jha et al. 2013). A better understanding of the causes of CKDu may be critical for health policies and public health responses. Previous studies have found that MPs/NPs accumulated in the gut, liver, and kidneys in mice (Deng et al. 2017b; Yang et al. 2019) and that they accumulated in seafood intended for human consumption (Smith et al. 2018). It is unclear whether polystyrene (PS)-MPs (PS-MPs) are risk factors in CKDu. MPs have been detected in many invertebrate species from the North Sea and in a subset of brown trout from the Swedish west coast (Karlsson et al. 2017). MPs pervade the global seafloor (Kane et al. 2020). In addition, PS is a popular plastic used worldwide (Hahladakis et al. 2018). Recently, PS-MPs have been found to induce several responses and to affect the physiological functions of various organisms. For example, one study showed that exposure of scleractinian coral species to PS-MPs regulated genes that are related to the stress response, zymogen granules, c-Jun N-terminal kinase (JNK) signaling pathways, sterol transport, and the epidermal growth factor (EGF)–extracellular signal-regulated kinase (ERK) one-half signaling pathway (Tang et al. 2018). PS-MPs induced oxidative stress in the livers of zebrafish (*Danio rerio*) (Lu et al. 2016) and mice (Deng et al. 2017b; Yang et al. 2019). Previous findings have also indicated that PS-MPs induced oxidative stress as the main mechanism of toxicity in other models (Barboza et al. 2018; Wu et al. 2019).

Mitochondria have central roles in glucose, fatty acid, and energy metabolism (Xu et al. 2020). Mitochondria also play important roles in oxidative stress and crosstalk in endoplasmic reticulum (ER) stress, the inflammasome, and autophagy in type 2 diabetes (Rocha et al. 2020). A previous study indicated that palmitic acid induced excessive mitochondrial reactive oxygen species (ROS) accumulation in podocytes (Jiang et al. 2020). Excessive mitochondrial ROS levels were associated with mitochondrial injury in mice with diabetic nephropathy (Hwang et al. 2012). Mice with diabetic kidney disease exhibited urinary albumin excretion (Han et al. 2018, 2019) Moreover, studies in dogs (Chacar et al. 2017) and cats (Ferlizza et al. 2017; Maeda et al. 2015) have shown that urinary proteins are one of the early biomarkers of CKD. In addition, the ER is an organelle with several essential functions, including protein synthesis and processing (Chen et al. 2010). Upon initiation of the unfolded protein response (UPR), ER stress is activated through three major signaling pathways: activating transcription factor 6 (ATF6), inositol-requiring enzyme 1α (IRE1α) and protein kinase RNA-activated (PRKR)-like ER kinase (PERK) pathways (Saito and Imaizumi 2018). In addition, PERK regulates eukaryotic initiation factor 2α (EIF2α) or phosphoinositide 3-kinase (PI3K)/AKT/mTOR signal pathway (Moretti et al. 2007). However, studies have revealed that ER stress is involved in various types of kidney diseases, including renal fibrosis, diabetic nephropathy, acute kidney injury, CKD, glomerulopathies associated with genetic mutations, and primary glomerulonephritis (Cybulsky 2017). CD36 has induced membrane calcium influx in response to ER stress, release of arachidonic acid from cytoplasmic phospholipase $A_2\alpha$ ($cPLA_2\alpha$), and generation of proinflammatory eicosanoids in Chinese hamster ovary cells (Kuda et al. 2011). Arachidonic acid is converted to prostaglandins through the cyclooxygenase (COX) pathway by the constitutive enzyme cyclooxygenase (COX)-1 or by inducible COX-2 in lung fibroblasts (Ghosh et al. 2004). Arachidonic acid metabolism is associated with kidney inflammation (Wang et al. 2019). In addition, autophagy is an important self-cleansing pathway (Mizushima 2018). Autophagy has been shown to maintain homeostasis of the glomeruli and tubules of mouse kidneys (Kimura et al. 2011) and has been implicated in cisplatin-induced kidney injury *in vitro* and *in vivo* (Bolisetty et al. 2010; Takahashi et al. 2012), senescence in mice (Hartleben et al. 2010; Liu et al. 2012), polycystic kidney disease (PKD) in mice (Belibi et al. 2011) and humans (Serra et al. 2010), and diabetic kidney disease in rats (Flaquer et al. 2010). Autophagy was also found to be necessary for stress adaptation in a mouse model of kidney injury, possibly because of its roles in removing protein aggregates and injured organelles and in promoting cell survival (Riediger et al. 2011). Autophagy-related markers such LC3, Beclin 1, and p62 are important participants in this process (Schmitz et al. 2016).

PS-MPs can damage the gut and liver of mice, and we found that a previous study has shown that PS-MPs accumulates in the kidneys in mice (Deng et al. 2017b; Yang et al. 2019). Another previous study also showed that PS-NPs (44 nm) were internalized via both endocytosis and diffusion in human renal cortical epithelial cells. PS-NPs did not affect cell viability, metabolism, or cell cycle progression. However, PS-NPs did accumulate in the perinuclear region (Monti et al. 2015). The studies that obtained these findings did not determine the kidney conditions after the accumulation of PS-MPs or PS-NPs. Thus far, the effects of MPs or NPs of the following sizes have been studied in mice: 0.025 μm (Rafiee et al. 2018), 0.05 μm (Rafiee et al. 2018), 0.5 μm (Deng et al. 2018; Lu et al. 2018; Luo et al. 2019b), 1 μm (Deng et al. 2018), 4 μm (Stock et al. 2019), 5 μm (Jin et al. 2019; Luo et al. 2019a, 2019b; Yang et al. 2019), 10 μm (Li et al. 2020; Stock et al. 2019), 20 μm (Deng et al. 2017b; Jin et al. 2019), 50 μm (Lu et al. 2018), and 150 μm (Li et al. 2020). Most of the studies had used PS. In the present study, we evaluated the effects of PS-MPs in HK-2 cells and male C57BL/6 mice. Mitochondrial ROS, ER stress, inflammation, and autophagy were analyzed in kidney cells. In mice, we evaluated kidney tissue histology and ultrastructure, biomarkers of kidney function, muscle mass, and grip strength, as well as PS-MP accumulation in the kidney tissue. Furthermore, we examined the possible mechanisms underlying the effects induced by PS-MPs.

Methods

Physicochemical Characterization

The 2-μm PS-MPs were obtained from Life Technologies (C37278). The average hydrodynamic size, polydispersity index (PDI) and zeta potential of the PS-MPs were determined by dynamic laser scattering (DLS) (Zetasizer Nano ZS90). Briefly, we used PS-MPs stock solution (4% wt/vol) to prepare a final concentration of 75-μg/mL PS-MPs solution in ultrapure water. The dilution method was 15 μL of PS-MPs stock solution added into 8 mL ultrapure water, then 1-mL aliquots of the well-mixed solution were placed into cuvettes and the solutions were analyzed with DLS in triplicate. The average hydrodynamic size, PDI, and zeta potential data were performed and directly output by Zetasizer Nano software (version 5.0) and these data were calculated using Microsoft Office Excel. The shapes and sizes of the PS-MPs were analyzed using transmission electron microscopy (TEM) with an H-7650 instrument (Hitachi). The PS-MPs were suspended in water, dropped onto copper-coated carbon grids, and dried overnight at room temperature prior to imaging. The actual sizes of the PS-MPs were measured using TEM software.

Cell Lines

The human kidney proximal tubular epithelial cell line HK-2 (ATCC CRL-2190) was obtained from the American Type Culture Collection (ATCC). The HK-2 cells were incubated and

maintained in keratinocyte–serum-free medium (SFM) with human recombinant EGF (rEGF) and bovine pituitary extract (BPE) (Life Technologies) at 37°C with 5% carbon dioxide (CO_2) and passaged every 2–3 d. Autophagy-related gene 5 (ATG5)-wild-type (WT; $Atg5^{+/+}$) and ATG5-knockout ($Atg5^{-/-}$) mouse embryonic fibroblasts (MEFs) were provided by N. Mizushima (Tokyo Medical and Dental University, Tokyo, Japan) (Kuma et al. 2004). The cells were cultured in Dulbecco's Modified Eagle's Medium Low Glucose (11885084; Life Technologies), supplemented with 10% fetal calf serum, penicillin (100 U/mL), and streptomycin (100 mg/mL) at 37°C with 5% CO_2 and passaged every 2–3 d.

Uptake of PS-MPs by HK-2 Cells

HK-2 cells (8×10^4) were seeded onto 12-mm glass slides (1001/12; GmH & Co. KG) in 24-well culture plates overnight and treated with 2 μm fluorescent yellow-green PS-MPs (L4530; Sigma-Aldrich) at concentrations of 0.025, 0.05, 0.1, 0.2, 0.4, or 0.8 μg/mL for 120 min or at a concentration of 0.8 μg/mL for 0, 5, 10, 30, or 60 min. Then, the slides were washed with phosphate-buffered saline (PBS) for 5 min, fixed with 4% paraformaldehyde for 15 min at room temperature, washed with tris-buffered saline containing 0.05% Tween-20 (TBS-T) for 10 min, stained with 0.1 mg/mL 4,6-dimidyl-2-phenylindole (DAPI) (D1306; Life Technologies) at room temperature for 10 min and mounted onto glass slides (0100-01; SouthernBiotech). Then, all slides were examined with a fluorescence microscope with an excitation filter (ECLIPSE Ci; Nikon). The fluorescent yellow-green PS-MPs spectra exhibited excitation and emission maxima of ∼470 and ∼505 nm, respectively. The excitation and emission wavelengths for the DAPI spectra were 360 nm and 460 nm, respectively. In addition, HK-2 cells (4×10^5) were treated with 0, 0.05, 0.1, 0.2, 0.4, or 0.8 mg/mL PS-MPs for 1 or 2 h. The cells were harvested with Accutase (AT-104; Innovative Cell Technologies), centrifuged at 1,200 rpm for 5 min at room temperature, washed with PBS, and suspended in PBS. The signal was measured using a flow cytometer (LSRFortessa; BD Biosciences) with *x*-axis for the side-scattered light (SSC) and *y*-axis for cell counts in histograms.

Lentivirus Knockdown

HK-2 cells (2×10^5) were seeded in 10-cm plates overnight. Lentivirus with control short hairpin RNA (shRNA; TRC1.Void) or *Atg5* shRNA#1 (CCGGCCTGAACAGAATCATCCTTAAC-TCGAGT-TAAGGATGATTCTGTTCAGGTTTTTTG, TRCN-0000151963) and *Atg5* shRNA#2 (CCGGCCTGAACAGAA-TCATCCTTAACTCGAGTTAAGGATGATTCTGTTCAGGT-TTTTG, TRCN0000330394) were purchased from the National RNAi Core Facility at Academia Sinica in Taiwan. Briefly, 8 μg/mL polybrene (sc-134,220; Santa Cruz) was mixed with lentivirus (multiplicity of infection = 3), which were then incubated in keratinocyte-SFM with human rEGF and BPE overnight at 37°C with 5% CO_2. The medium was changed after 24 h, 2 μg/mL puromycin (ant-pr-1; InvivoGen) was added, and incubation was continued for 72 h. Stable ATG5 knockdown ($ATG5^{KD}$) HK-2 cells were constructed after puromycin selection. The $ATG5^{KD}$ HK-2 cells were incubated and maintained in keratinocyte-SFM with human rEGF and BPE at 37°C with 5% CO_2 and passaged every 2 or 3 d.

Cell Viability Assay

Cell viability was assessed with a sulforhodamine B (SRB; Sigma) assay. SRB can bind to basic amino acids in proteins. The amount of dye represents the number of cells. Briefly, cells (4×10^3) were seeded in a 96-well culture plate and incubated overnight at 37°C. HK-2 cells were treated with PS-MPs (Life Technologies) at 0, 0.05, 0.1, 0.2, 0.4, or 0.8 mg/mL for 1, 2, or 3 d. The cells were fixed with ice-cold 10% trichloroacetic acid (TCA; Sigma) at 4°C for at least 1 h or overnight. The TCA was removed, and the cells were washed twice with distilled water. Then, 0.1% SRB in 1% acetic acid (Sigma) was added, and the cell suspension was incubated at 25°C for 1 h. The cells were washed twice with 1% acetic acid and dried at 60°C in an oven for 30 min. Finally, the adhered cells were dissolved in 20 mM Tris base buffer (Sigma), and the plate was shaken for 30 min. The absorbance of the dye suspension was measured at a wavelength of 562 nm in an enzyme-linked immunosorbent assay (ELISA) reader (EMax Plus; Molecular Devices).

Apoptosis and Necrosis Analysis

Cells (4×10^5) were treated with PS-MPs at 0, 0.05, 0.1, 0.2, 0.4, or 0.8 mg/mL for 24 or 48 h. The cells were harvested with Accutase (Innovative Cell Technologies), centrifuged at 1,200 rpm, and washed with PBS. Apoptosis and necrosis were quantified using a fluorescein isothiocyanate (FITC) Annexin V/propidium iodide (PI) apoptosis detection kit according to the manufacturer's protocol (640914; BioLegend). Briefly, 5 μL FITC Annexin V was added, 10 μL PI solution was added, and the cells were vortexed gently and incubated for 15 min at room temperature in the dark. Finally, 400 μL Annexin V binding buffer was added to each tube to stop the reaction. The signal was measured using a flow cytometer (BD Biosciences). The excitation and emission wavelengths for the FITC Annexin V spectra were 490 nm and 525 nm, respectively. A 488 nm-laser was used for excitation. The apoptotic index was presented as the percentage of Annexin V^+PI^+ and Annexin V^+PI^- cells in the four quadrants. The necrotic index is presented as the percentage of Annexin V^-PI^+ cells in the four quadrants.

Western Blot Analysis

HK-2 cells (4×10^5) were seeded in 6-well culture plates and incubated overnight at 37°C. The cells were treated with PS-MPs at 0, 0.05, 0.1, 0.2, 0.4, or 0.8 mg/mL for 5 min, 10 min, 15 min, 30 min, 60 min, 24 h, or 48 h. Radioimmunoprecipitation assay buffer [25 mM Tris-hydrochloride (pH 7.6), 150 mM sodium chloride, 1% nonyl phenoxypolyethoxylethanol (NP-40), 1% sodium deoxycholate, 0.1% sodium dodecyl sulfate (SDS)] with a protease inhibitor cocktail (11873580001; Roche) and phosphatase inhibitor (PIC009; Bioshop) was added to each well, and the lysates were collected. The cell lysates were subjected to three cycles of 30 s of vortexing and 30 s of cooling, and then centrifuged at $13,000 \times g$ for 30 min. The supernatant was taken for protein quantification with a Bradford protein assay (500-0006; Bio-Rad) and measured at a wavelength of 595 nm in an ELISA reader (Molecular Devices). Proteins (20–50 μg) were boiled for 5 min in SDS sample buffer [62.5 mM Tris (pH 6.7), 1.25% SDS, 12.5% glycerol, and 2.5% β-mercaptoethanol]. The proteins isolated from the cells and TD-PM10315 TOOLS Pre-Stained Protein Marker (10–315 kDa) (BIOTOOLS Co., Ltd.) were loaded onto gradient gels for SDS–polyacrylamide gel electrophoresis (PAGE) (TFU-GG420; BIOTOOLS). After transfer to a 0.45-μm nitrocellulose membrane (GE10600002; Amersham), the proteins on the membrane were blocked with 5% skim milk (70166; Sigma) in TBS-T for 1 h and incubated with antibodies overnight at 4°C. Antibodies against phospho-eukaryotic initiation factor 2 alpha (p-EIF2α (3398, 1:1,000), EIF2α (5324, 1:2,000), IRE1α (3294; 1:1,000), COX-1 (4841; 1:1,000), p-p38 (9211; 1:1,000), p38 (9212; 1:1,000), p-ERK1/2 (9101; 1:1,000), ERK1/2 (4695; 1:1,000), p-JNK

(9251; 1:1,000), JNK (9252; 1:1,000), p-mTOR (2971; 1:1,000), mTOR (2983; 1:1,000), p-AKT (9275; 1:1,000), AKT (4685; 1:1,000), Beclin 1 (3738; 1:1,000), and Bad (9292; 1:1,000) were obtained from Cell Signaling Technology. Antibodies against ATF6 (24169-1; 1:1,000), Bcl2 (12789-1; 1:1,000), glyceraldehyde 3-phosphate dehydrogenase (GAPDH; 60004-1; 1:200,000), and Bax (50599-2-Ig; 1:3,000) were obtained from Proteintech. An antibody against $cPLA_2$ (sc-545, 1:500) was obtained from Santa Cruz Biotechnology; antibodies against p62 (PM045, 1:1,000) and LC3 (PM036, 1:1,000) were obtained from MBL International. The primary antibodies were washed from the membrane with TBS-T for 15 min three times at room temperature. The membrane was then incubated with antimouse (111-035-003; 1:1,000; Jackson) or antirabbit (111-035-003; 1:1,000; Jackson) secondary antibody for 2 h and washed with TBS-T for 15 min three times at room temperature. For phosphoprotein detection, the antibodies were stripped (TW-ST500; TOOLStripping Buffer; TOOLS) from the membrane at 37°C for 10 min. The membrane was then washed with a large amount of water and with TBS-T twice and reprobed for total antibody binding. The immunoreactive bands were visualized using an enhanced chemiluminescence (ECL) system (Amersham). Protein expression was quantified with ImageQuant (version 5.1; GE Healthcare). The band of western blot was quantified to normalize the total protein or GAPDH. Figures S2–S9 show the quantification of western blot and graph of the mean ± standard deviation (SD).

Immunostaining Assay

HK-2 cells (8×10^4) were seeded on 12-mm glass slides (GmH & Co. KG) in 24-well culture plates and treated with PS-MPs. After fixing the cells in 4% paraformaldehyde for 15 min, the slides were washed in PBS. Bovine serum albumin (BSA; 3%) was added to the slides, and the slides were incubated for 30 min. The slides were then incubated with the LC3 antibody (MBL; 1:200) diluted in 3% BSA at 4°C overnight and washed in TBS-T for 15 min three times. Then, the slides were incubated with a secondary antibody (111-095-003; 1:200; Jackson) labeled with FITC for 2 h at room temperature. Finally, the slides were stained with 0.1 mg/mL DAPI (Life Technologies) at room temperature for 10 min and mounted on glass slides (0100-01; SouthernBiotech). Then, all slides were examined with a fluorescence microscope with an excitation filter (Nikon) or a Leica TCS SP5 confocal microscope (Leica Microsystems). The fluorescence intensity was examined in three fields of view (>100 cells/field). The excitation and emission wavelengths for the FITC spectra were 490 nm and 525 nm, respectively. The excitation and emission wavelengths for the DAPI spectra were 360 nm and 460 nm, respectively.

Measurement of Mitochondrial ROS Production

HK-2 cells (8×10^4) were seeded on 12-mm glass slides (GmH & Co. KG) in 24-well culture plates overnight; treated with PS-MPs at 0.025, 0.05, 0.1, 0.2, 0.4, or 0.8 μg/mL; and harvested after 6 h. MitoTEMPO, a mitochondrial ROS antioxidant (SML0737; Sigma) (Cai et al. 2016) was used at 40, 80 or 100 μM and treated with PS-MPs with 0.8 μg/mL or not in HK-2 cells. Mitochondrial ROS levels were analyzed via treatment of the cells in 5 μM MitoSOX Red (M36008; Life Technologies) for 10 min at 37°C. Then the cells were washed with PBS three times, fixed with 4% paraformaldehyde for 15 min, washed with PBS for 5 min, stained with 0.1 mg/mL DAPI (Life Technologies) for 10 min, and mounted on glass slides (SouthernBiotech) at room temperature. Images of MitoSOX Red fluorescence were collected using a fluorescence microscope with an excitation filter (Nikon). The spectra for MitoSOX Red showed excitation and emission maxima of ~510 and 580 nm, respectively. The excitation and emission wavelengths for the DAPI spectra were 360 nm and 460 nm, respectively. The fluorescence intensity was examined in three fields of view (>50 cells/field). The fluorescence was analyzed and quantified with TissueQuest (TissueGnostics GmbH) to quantify the fluorescence of MitoSOX Red-positive cells. Briefly, the files were selected, and the red and blue fluorescence was separated. The dimensions were $1,080 \times 1,024$ pixels, the resolution was ~96 dpi, the bit depth was 8, and the color representation was uncalibrated. The data were then analyzed.

Animal Model

Six-week-old male C57BL/6 mice were obtained from the National Laboratory Animal Center in Taiwan and were maintained in compliance with institutional policy. All animal procedures were approved by the institutional animal care and use committee at Taipei Medical University (approval no. LAC-2019-0520). The mice were raised in an animal center room with a 12-h light/dark cycle and 55% ± 10% relative humidity at 22 ± 2°C. A previous study has shown that a regime of 0.1 mg/d of 5 μm and 20 μm PS-MPs (once daily by oral gavage) accumulated PS-MPs in the mouse kidneys for 4 wk (Deng et al. 2017b). In this experiment, PS-MPs were diluted in distilled water, and mice were administered the PS-MPs by oral gavage at 0.2 mg/d and 0.4 mg/d twice per week for 4 or 8 wk. The mice in the sham group received water. The mice were randomized into three groups of five mice each. If the veterinarian advised it or if the weight loss of a mouse was more than 15%, the mouse was humanely euthanized before the end of the experiments. Otherwise, the mice were humanely euthanized via CO_2 exposure at the end of the experiments, and their kidneys and leg muscles were obtained and fixed with 10% formalin for further histological analysis. Urine was collected directly into 1.5-mL sterile Eppendorf tubes from the mice the day before they were euthanized at the end of the experiments. The mice used for urine collection were not raised in segregated cages during the experiments.

Biochemical Evaluation

Mice were randomized into three groups of five mice each and treated at 0.2 mg/d or 0.4 mg/d twice per week for 4 or 8 wk. The mice in the sham group received water. Whole-blood samples were collected from the sham and treated mice by intracardiac puncture immediately after the mice were euthanized. Then, the blood samples were left to stand for 30 min and centrifuged at $2,000 \times g$ for 20 min to separate the serum. Biochemical indices including blood urea nitrogen (BUN) levels (417-65291; Wako) and creatinine levels (1875418; Roche), were tested using a Hitachi 7080 analyzer by the National Laboratory Animal Center in Taiwan.

SDS-PAGE and Western Blot Analysis

Urine samples from different mice were centrifuged at $1,200 \times g$ for 10 min, and 8 μL of each sample was dissolved in the sample buffer [62.5 mM Tris (pH 6.7), 1.25% SDS, 12.5% glycerol, and 2.5% β-mercaptoethanol] for loading. Briefly, urine samples were boiled for 5 min in the sample buffer for loading of protein. The urine samples and HR Pre-Stained Protein Markers (10-170 kDa) (161-0374; Bio-Rad) were loaded onto gradient SDS-PAGE gels (BIOTOOLS) and subjected to electrophoresis. The gel was stained with Coomassie blue (TTD-BS1L; TOOLStart Blue Staining Reagent; BIOTOOLS) for 30 min and destained with water for 10 min. The gel was scanned with an SCX-3405 scanner (Samsung). The samples were analyzed using SDS-PAGE. After transfer to a nitrocellulose membrane (Amersham), the

proteins were incubated with an anti-albumin antibody (1:1,000; GTX102419; GeneTex). The subsequent steps were conducted as described previously. Western blotting was performed with a separate gel. The immunoreactive bands were visualized using an enhanced chemiluminescent (ECL) Western Blotting Detection Reagents (RPN2235, Amersham).

PS-MP Detection with Raman Spectra in Kidney Tissues

Mice were administered PS-MPs by oral gavage at 0.4 mg/d twice per week for 8 wk. The mice in the sham group received water. There were five mice in each group. The mice were humanely euthanized via CO_2 exposure at the end of the experiments, and one kidney was obtained from each mouse. To prepare a standard curve for calibration, 10 mg of ground tissues from the control group were mixed with different concentrations of PS-MPs to prepare samples with 0, 0.4, 1.6, 4, and 8 mg/g_{kidney}. The powders were dried in a desiccator with a vacuum system. The dried samples were further measured with a micro-Raman system. Raman spectra were acquired by using a Jobin–Yvon LabRAM high-resolution Raman spectrometer (Horiba iHR 320) and a 785-nm laser (DPSSL Driver II; 10 mW), integrated with an Olympus BX53 microscope.

Tubular Injury Analysis

One kidney from each mouse was fixed in 10% formalin for 24 h and embedded with Shandon HistoCentre 3 (Thermo), sectioned at 2-μm thickness with a Leica microtome (RM2245), and stained with hematoxylin and eosin (H&E) for histological analyses. The tubular injury rate was examined in 20 fields of view per kidney (5 mice per group). The severity of tubular damage was scored from 0 to 5 according to morphological changes in the tubular lesion area, such as tubular dilatations, loss of brush borders, and flattening of the tubular epithelia. The tubular damage index (TDI) was assessed as follows: 0, normal; 1, area of tubular dilation and brush border attenuation involving <10% of the field of view; 2, lesion area between 10% and 20% of the field of view; 3, lesion area between 20% and 30% of the field of view; 4, lesion area between 30% and 40% of the field of view; and 5, lesion area >40% of view. The tubular injury rates were analyzed in a blinded manner.

Immunohistochemistry

The sections were placed in an oven (60°C) for 1 h. The sections were washed twice with xylene (Sigma) for 10 min each, twice with 100% ethyl alcohol (Sigma) for 10 min each, once with 95% ethyl alcohol for 5 min, and once with 75% ethyl alcohol for 5 min. For immunostaining, the sections were boiled with citrate buffer solution [0.01 M (pH 6.0), with 1% Tween 20] for 30 min. Immunohistochemistry (IHC) consumables and reagents from Thermo Scientific (Life Technologies) were used according to the protocol. Briefly, the sections were blocked with hydrogen peroxide (TA-060-H202Q; Thermo Scientific) for 10 min, washed with TBS-T for 15 min three times, and blocked UltraVision protein block (TL-060-QHL; Thermo Scientific) for 10 min at room temperature. The slides were incubated with antibodies against IRE1α (1:500; NB100-2,324; Novusbio), LC3 (1:2,000; MBL), COX-1/PTGS1 (1:1,000; A7341; ABclonal Technology), or dystrophin (1:100; sc-73592; Santa Cruz) in 3% BSA overnight at 4°C, and washed with TBS-T for 15 min three times at room temperature. The slides were hybridized with a primary antibody amplifier quanto (TL-060-QHL; Thermo Scientific) for 10 min, washed with TBS-T for 15 min three times, hybridized with a horseradish peroxidase (HRP) polymer quanto (TL-060-QHL; Thermo Scientific) for 10 min, and washed with TBS-T for 15 min three times at room temperature. The slides were stained with 3,3′-diaminobenzidine (DAB; TA-060-QHDX; Thermo Scientific), the reactions were stopped with water, and the sections were counterstained with hematoxylin (HMM500; ScyTek) at room temperature for 3 min. For Masson's trichrome staining (TRM-2-IFU, ScyTek), a kit was used according to manufacturer's to the protocol. Finally mounting medium was added to the slides, and coverslips were mounted. Once the mounting medium solidified, the sections were scanned with Motic Digital Slide Assistant (Motic VM3.0). The images were analyzed with ImageJ plugins to quantify the positive cells (Papadopulos et al. 2007). The IHC of positive percentage areas were examined in 10 fields of view.

Transmission Electron Microscopy

Six-week-old male C57BL/6 mice received PS-MPs by oral gavage at 0.4 mg/d twice per week for 8 wk. The mice were treated about 1 wk after they arrived. The mice in the sham group received water. For the qualitative experiment, the mice were randomized into two groups of three mice per group. The mice were humanely euthanized via CO_2 exposure at the end of the experiments, and their kidneys were obtained after perfusion (0.1 M PBS) and fixation [0.1 M PBS, 4% paraformaldehyde, 0.1% glutaraldehyde (pH 7.4)] with a Masterflex peristaltic pump (7518-00) with flow rate for 1 drop/s of ∼20 mL. The kidney tissues were embedded in EPON resin (13940; Electron Microscopy Sciences), sectioned into 60-nm-thick sections, and observed under an HT7700 (Hitachi) transmission electron microscope. In detail, the samples were washed with 0.1 M cacodylate (205541; Merck) for 15 min three times; postfixed in 1% osmium tetroxide (Ubichem) for 1–2 h; treated with 0.1 M cacodylate for 15 min three times; washed in 70%, 80%, 90%, 95%, and 100% alcohol for 15 min per wash; incubated in propylene oxide (PO; 110205; Sigma) for 10 min; incubated in 1:1 PO/EPON resin overnight with vacuum under 50 cmHg; incubated in EPON resin for another 8 h, placed in an oven at 62°C for 48–72 h, and finally sectioned with an ultramicrotome (EM UC7; Leica).

Forelimb Grip Strength Test

Six-week-old male C57BL/6 mice received PS-MPs by oral gavage at 0.4 mg/d twice per week for 8 wk. The mice were treated about 1 wk after they arrived. The mice in the sham group received water. For function analysis, the mice were randomized into two groups of seven mice per group. A conventional hand-grip strength meter (Digitech; DTG-2) was used (Takeshita et al. 2017). Briefly, the grip strength meter was changed to the peak model and reset to 0 kgf. Then, the inspector allowed a mouse to grasp a bar mounted on the force gauge, and the mouse's tail was gently pulled back until the mouse released the bar. The grip strength meter thus recorded the maximum force of the mouse's forelimb grip. The order in which the mice were tested was randomized, and the inspector was blinded to the results of the previous tests.

Statistical Analysis

The data were analyzed with GraphPad Prism (version 8.4.3; GraphPad Software) and are expressed as the means ± SDs. The data were analyzed by *t*-test, one-way analysis of variance (ANOVA), and two-way ANOVA according to groups; Dunnett's multiple comparison test, Sidak's multiple comparisons test, and Tukey's multiple comparisons test were used for further comparisons between groups. Statistical significance was determined at $p < 0.05$. The actual *p*-values for the nonsignificant and significant results are shown in Table S4.

Results

PS-MP Characterization

PS-MPs with a primary particle size of 2 μm were purchased from Life Technologies. The detailed physicochemical characteristics of the PS-MPs after suspension in water are summarized in Table S1. The hydrodynamic diameter of the PS-MPs was 1.878 ± 0.677 μm. The zeta potential of the PS-MPs was -76 ± 1.2 mV. The PDI for the PS-MPs was 0.189. Furthermore, the TEM images suggested that the PS-MPs were mostly spherical in shape (Figure S1).

Uptake of PS-MPs by HK-2 Cells

The effects of different concentrations of PS-MPs were investigated after 2 h. As shown in Figure 1A, fluorescence analysis revealed that 0.8 mg/mL PS-MPs resulted in the most obvious effects. When the effects of 0.8 mg/mL PS-MPs over different uptake durations were investigated, fluorescence analysis revealed that a 60-min uptake time produced the most obvious effects (Figure 1B). As shown in Figure 1C,D, among different concentrations of PS-MPs, the 0.8-mg/mL concentration had the most obvious effects after uptake for 1 h (0-mg/mL group vs. 0.4-mg/mL group, $p = 0.0025$; 0-mg/mL group vs. 0.8-mg/mL group, $p < 0.001$) or 2 h (0-mg/mL group vs. 0.2-mg/mL group: $p = 0.0039$; 0-mg/mL group vs. 0.4-mg/mL group: $p < 0.001$; 0-mg/mL group vs. 0.8 mg/ml group: $p = 0.001$). The mean and SD summary data for quantification are shown in Table S3. SSC showed a shift in peak from left to right in a concentration-dependent manner. The SSC data were used to identify cellular granularity. HK-2 cells treated with PS-MPs at 0.8 mg/mL took up $\sim 3.55 \pm 0.6$ times more PS-MPs than the control cells at 2 h.

Cell Viability, Mitochondrial ROS, and Expression of Apoptosis-Related Protein in HK-2 Cells Treated with PS-MPs

As shown in Figure 2A, the cell viability of cells treated with PS-MPs was similar to those treated with the water control. None of the treated groups had significant differences except on Day 3 (0-mg/mL group vs. 0.8-mg/mL group: $p = 0.0241$) (Tables S3 and S4). The necrosis index was significantly different between the control group and the 0.4- or 0.8-mg/mL groups, and it was $\sim 10\%$ in both of these groups compared with $\sim 5\%$ in the control (0-mg/mL group vs. 0.4-mg/mL group: $p = 0.0319$; 0-mg/mL group vs. 0.8-mg/mL group: $p = 0.0026$) (Figure 2B,C). The mean and SD summary data for quantification of western blots are shown in Table S3. However, the apoptosis index did not significantly differ among groups (Figure 2B,C). HK-2 cells treated with PS-MPs at different concentrations exhibited higher mitochondrial ROS levels (Figure 2D). Specifically, cells treated with 0.2, 0.4, or 0.8 mg/mL PS-MPs had significantly higher mitochondrial ROS levels (0-mg/mL group vs. 0.2-mg/mL group: $p = 0.0331$; 0-mg/mL group vs. 0.4-mg/mL group: $p < 0.001$; 0-mg/mL group vs. 0.8-mg/mL group: $p < 0.001$), and the fold-change in the 0.8-mg/mL group compared with the control group was 3 ± 0.6 times (Figure 2E). In addition, the expression of Bad, which is associated with mitochondrial-mediated apoptosis regulation, was significantly higher after treatment of HK-2 cells with 0.8-mg/mL PS-MPs for 5–60 min in HK-2 cells (Figure 2F and Figure S2). The expression of Bcl2, which is also associated with mitochondrial-mediated apoptosis regulation, was significantly lower after treatment of HK-2 cells with 0.8-mg/mL PS-MPs for 20–60 min in HK-2 cells (Figure 2G and Figure S2). However, the expression of Bax, which is also associated with mitochondrial-mediated apoptosis regulation, was not significantly changed after PS-MPs treatment of HK-2 cells (Figure 2H and Figure S2).

Expression of Proteins Related to ER Stress, Inflammation, and Autophagy in HK2 Cells Treated with PS-MPs

As shown in Figure 3A and Figure S3, cells exposed to PS-MPs at different concentrations for 24 h had higher expression of the ER stress-related protein IRE1α. Therefore, the expression of other ER stress-related proteins ATF6 and the p-EIF2α/EIF2α ratio were not significantly different. In addition, the phosphorylation of MAPK signaling molecules, such as p38, ERK1/2, and JNK was higher in treated cells compared with control (Figure 3B and Figure S4). Specifically, p-p38, p-ERK1/2, and p-JNK levels were highest at 10–30 min after exposure. Cells exposed to PS-MPs also exhibited higher expression of inflammation-related proteins such as $cPLA_2$ and COX-1. Specifically, $cPLA_2$ expression was significantly higher after treatment with 0.8-mg/mL PS-MPs (0-mg/mL group vs. 0.8-mg/mL group: $p = 0.0171$ (Figure 3C and Figure S5). COX-1 expression was significantly higher in cells exposed to 0.4-mg/mL PS-MPs (0-mg/mL group vs. 0.4-mg/mL group: $p = 0.0284$; 0-mg/mL group vs. 0.8-mg/mL group: $p = 0.023$) (Figure 3C and Figure S5). In contrast, cells exposed to PS-MPs had lower levels of phosphorylation in AKT/mTOR signaling pathway components, such as mTOR and AKT, in a concentration-dependent manner in HK-2 cells (Figure 3D and Figure S6). Cells exposed to PS-MPs exhibited higher expression of autophagy-related protein LC3 and Beclin 1. The expression of p62 was not significantly different with increasing PS-MPs concentration. Moreover, LC3-II levels were higher in a concentration-dependent manner (Figure 3E and Figure S7). Expression of LC3 in HK-2 cells following exposure to PS-MPs was also concentration-dependent (Figure 3F). Specifically, cells treated with PS-MPs at 0.1 to 0.8 mg/mL had significantly higher LC3 expression as determined by immunofluorescence (0-mg/mL group vs. 0.1-mg/mL group: $p = 0.0265$; 0-mg/mL group vs. 0.2-mg/mL group: $p < 0.001$; 0-mg/mL group vs. 0.4-mg/mL group: $p < 0.001$; 0 mg/mL group vs. 0.8-mg/mL group: $p < 0.001$). Approximately $22.61 \pm 3.8\%$ of HK-2 cells treated with 0.8-mg/mL PS-MPs expressed LC3 signals (Figure 3G). The mean and SD summary data for quantification of Figure 3G are shown in Table S3.

Mitochondrial ROS in HK-2 Cells Exposed to PS-MPs and Treated with or without MitoTEMPO Superoxide Dismutase

As shown in Figure 4A,B, cells treated with 100 μM MitoTEMPO and exposed to PS-MPs had less mitochondrial ROS than those treated with PS-MP alone (0.8 mg/mL), with a reading of $295.5 \pm 21.5\%$ for PS-MPs alone and $169.4 \pm 9.6\%$ for PS-MPs with 100 μM MitoTEMPO (0.8-mg/mL PS-MP group vs. 0-mg/mL group: $p = 0.0019$; 0.8-mg/mL PS-MP group vs. 0.8-mg/mL PS-MP+100 μM MitoTEMPO group: $p = 0.0135$). Bad expression was significantly lower after PS-MP and MitoTEMPO treatment than with PS-MP treatment alone (Figure 4C and Figure S8A). Similar to Bad expression, IRE1α expression (Figure 4D and Figure S8B), and LC3-II expression, was lower after PS-MP and MitoTEMPO treatment than with PS-MP treatment alone (Figure 4G and Figure S8E). The phosphorylation of mTOR was significantly higher after PS-MP and MitoTEMPO treatment (Figure 4F and Figure S8D) compared with PS-MP treatment alone. However, ERK1/2 phosphorylation did not differ in cells treated with PS-MP and MitoTEMPO (Figure 4E and Figure S8C) compared with PS-MP exposure alone.

Cell Viability in ATG5 HK-2 Knockdown Cells and ATG5 MEF KO Cells Treated with PS-MPs

As shown in Figure 5A, an $ATG5^{KD}$ HK-2 cell line was constructed and tested. The results showed that ATG5 protein expression was lower in the knockdown cells than in the control cells. $ATG5^{KD}$

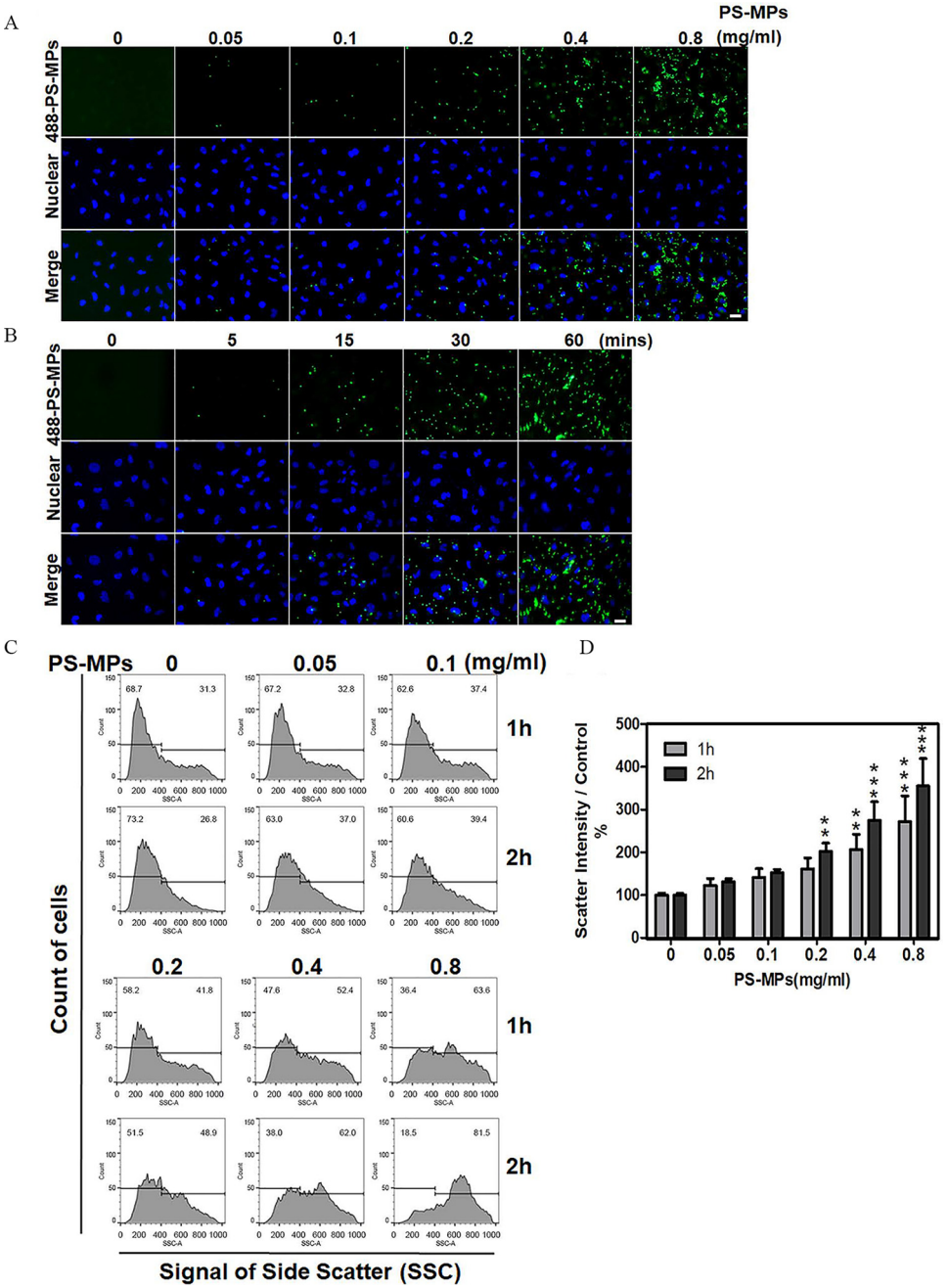

Figure 1. Uptake of PS-MPs by HK-2 cells. (A) Cells were treated with PS-MPs (yellow-green fluorescence) at concentrations of 0.05, 0.1, 0.2, 0.4, and 0.8 mg/mL for 2 h. Scale bar: 20 μm. (B) Cells were treated with 0.8-mg/mL PS-MPs (yellow-green fluorescence) for 0, 5, 15 30, and 60 min. DAPI (blue) was used for nuclear staining. Scale bar : 20 μm. (C) Cells were treated with PS-MPs at concentrations of 0.05, 0.1, 0.2, 0.4, and 0.8 mg/mL for 1 and 2 h and analyzed by flow cytometry. (D) Scatter intensity signals were graphed and analyzed after treatment with PS-MPs at concentrations of 0.05, 0.1, 0.2, 0.4, and 0.8 mg/mL for 1 and 2 h. $n = 3$. $^{**}p < 0.01$ and $^{***}p < 0.001$ compared with the control group, as determined by two-way ANOVA with Sidak's multiple comparisons test. Significance at 1 h: 0-mg/mL group vs. 0.4-mg/mL group: $p = 0.0025$, 0-mg/mL group vs. 0.8-mg/mL group: $p < 0.001$); 2 h: 0-mg/mL group vs. 0.2-mg/mL group: $p = 0.0039$; 0-mg/mL group vs. 0.4-mg/mL group: $p < 0.001$; 0-mg/mL group vs. 0.8-mg/mL group: $p < 0.001$. The data are presented as the means ± SDs. The mean and SD summary data for quantification of (D) are shown in Table S3. *p*-Values for all comparisons in (D) are reported in Table S4. Note: DAPI, 4,6-dimidyl-2-phenylindole; HK-2 cells, human kidney 2 cells; PS-MPs, polystyrene microplastics; SSC, side scatter light; SD, standard deviation.

HK-2 cells treated with PS-MPs had ~20–30% lower cell viability than control cells treated with PS-MPs. Treatment with 0.8-mg/mL PS-MPs reduced the viability in the two knockdown lines, $ATG5^{KD}$#1 and $ATG5^{KD}$#2, to 75.6 ± 2.2% and 66.6 ± 13.6%, respectively ($ATG5^{KD}$#1: 0-mg/mL group vs. 0.4-mg/mL group: $p = 0.0174$, 0-mg/mL group vs. 0.8-mg/mL group: $p = 0.0047$; $ATG5^{KD}$#2: 0-mg/mL group vs. 0.4-mg/mL group: $p < 0.001$, 0-mg/mL group vs. 0.8-mg/mL group, $p < 0.001$) (Figure 5B). The levels of ATG5 and LC3-II were lower after PS-MPs were added to the $ATG5^{KD}$ HK-2 cells. However, COX-1 expression was higher (Figure 5C and Figure S9). The cells therefore showed knockdown of ATG5 expression and higher COX-1 protein expression. $Atg5^{-/-}$ MEFs exposed to PS-MPs had higher levels of cell death; the viability in $Atg5^{-/-}$ MEF cells treated with 0.4-mg/mL or 0.8-mg/mL PS-MPs was 84.5 ± 4.9 or 65.6 ± 7.4% of that the control cells, respectively (Figure 5D). $Atg5^{+/+}$ MEF cells vs. $Atg5^{-/-}$ MEFs: 0.4-mg/mL group, $p = 0.0321$; 0.8-mg/mL group, $p < 0.001$). Furthermore, in $Atg5^{+/+}$ MEFs, the apoptosis index was

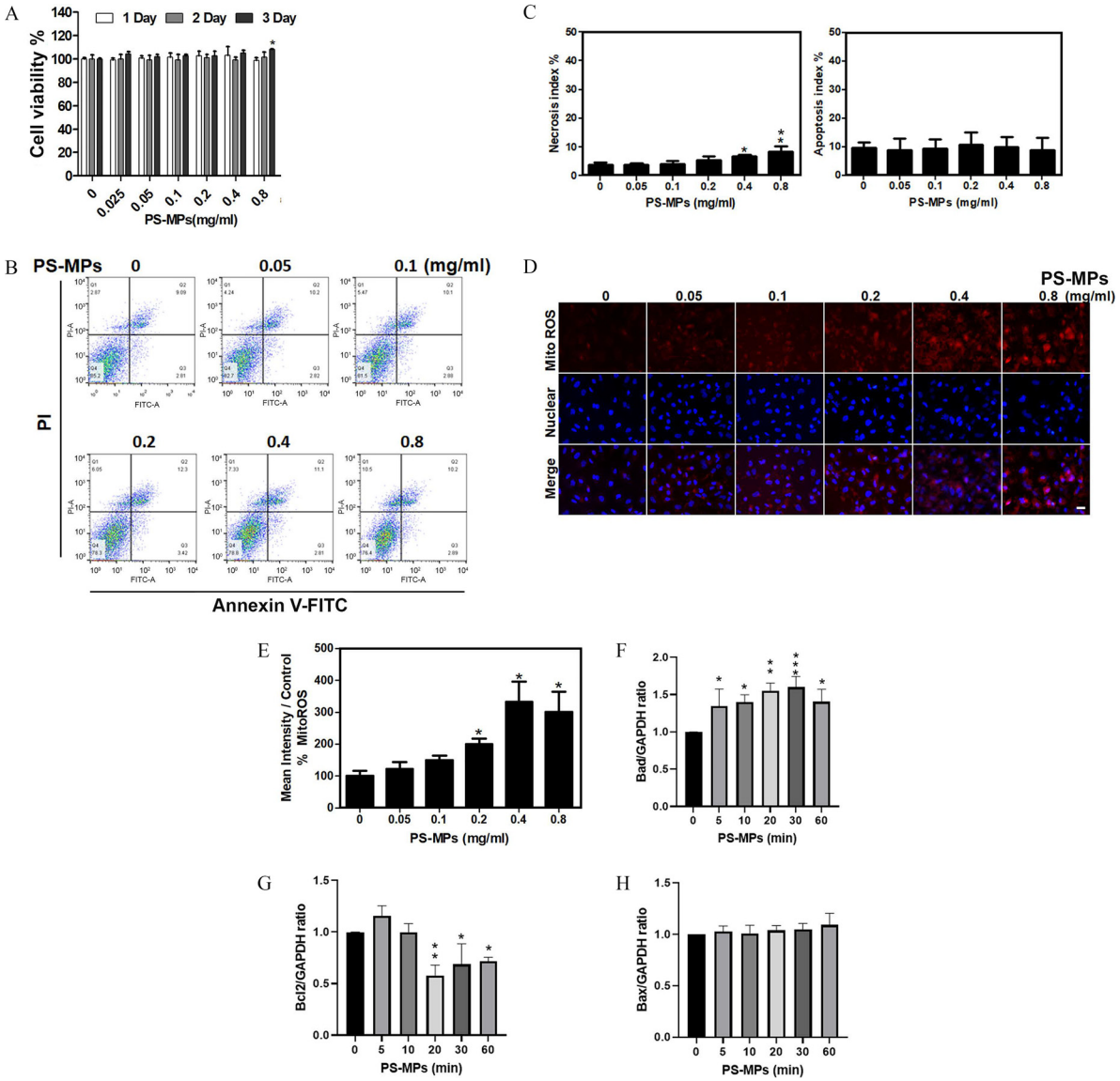

Figure 2. Cell viability, apoptosis, necrosis, mitochondrial ROS levels, and apoptosis-related proteins expression in HK-2 cells treated with PS-MPs. (A) Cell viability was determined after treatment with PS-MPs at concentrations of 0.05, 0.1, 0.2, 0.4, and 0.8 mg/mL for 1, 2, and 3 d. $n=3$. $^{*}p<0.05$ compared with the control group, as determined by two-way ANOVA with Dunnett's multiple comparisons test. Significance: Day 3, 0-mg/mL group vs. 0.8-mg/mL group: $p=0.0241$. The mean and SD summary data of (A) are shown in Table S3. For all p-values, see Table S4. (B) Apoptosis was detected by flow cytometry after treatment with PS-MPs at concentrations of 0.05, 0.1, 0.2, 0.4, and 0.8 mg/mL for 24 h. (C) The necrosis and apoptosis indexes were graphed and analyzed. $n=3$. $^{*}p<0.05$ and $^{**}p<0.01$ compared with the control group, as determined by one-way ANOVA with Dunnett's multiple comparison test. Significance: necrosis index: 0-mg/mL group vs. 0.4-mg/mL group: $p=0.0319$, 0-mg/mL group vs. 0.8-mg/mL group: $p=0.0026$; apoptosis index: no significant differences (Table S4). The mean and SD summary data of (C) are shown in Table S3. (D) Mitochondrial ROS were detected with 5 μM MitoSOX Red after treatment with PS-MPs at concentrations of 0.05, 0.1, 0.2, 0.4, and 0.8 mg/mL for 6 h. DAPI (blue) was used for nuclear staining. Scale bar: 20 μm. (E) Mitochondrial ROS levels were graphed and statistically analyzed. $n=2$. $^{*}p<0.05$ and $^{***}p<0.001$ compared with the control group, as determined by one-way ANOVA with Dunnett's multiple comparison test. Significance: 0-mg/mL group vs. 0.2-mg/mL group: $p=0.0331$, 0-mg/mL group vs. 0.4-mg/mL group: $p<0.001$, 0-mg/mL group vs. 0.8-mg/mL group: $p=0.001$. The mean and SD summary data of (E) are shown in Tables S3 and S4. The levels of apoptosis-related proteins, such as (F) Bad, (G) Bcl2, and (H) Bax, were assessed after treatment with PS-MPs at a concentration of 0.8 mg/mL for 0, 5, 10, 20, 30, and 60 min. GAPDH served as an internal control. The data are presented as the means ± SDs. The mean and SD summary data for quantification of western blots are shown in Table S3. The western blotting results were quantified and statistically analyzed as shown in Figure 2. Note: ANOVA, analysis of variance; DAPI, 4,6-dimidyl-2-phenylindole; GAPDH, glyceraldehyde 3-phosphate dehydrogenase; HK-2 cells, human kidney 2 cells; PS-MPs, polystyrene microplastics; ROS, reactive oxygen species; SD, standard deviation.

19.7 ± 2.4 or 25.1 ± 1.8 after treatment with 0.4-mg/mL or 0.8-mg/mL PS-MPs, respectively (Figure 5E,F). In $Atg5^{-/-}$ MEFs, the apoptosis index was 27.5 ± 2.4 or 36.9 ± 4.5 after treatment with 0.4-mg/mL or 0.8-mg/mL PS-MPs, respectively. The apoptosis index was significantly higher in a concentration-dependent manner in $Atg5^{-/-}$ MEF cells compared with $Atg5^{+/+}$ MEF cells ($Atg5^{+/+}$ MEF cells vs. $Atg5^{-/-}$ MEFs: 0.4-mg/mL group, $p=0.0426$; 0.8-mg/mL group, $p=0.003$). However, the necrosis index did not show any significant differences (Figure 5F and Table S4).

Body Weight, BUN and Creatinine Levels, and Tubule Characterization of Mice Treated with PS-MPs

As shown in Figure 6A, body weight did not significantly differ between mice that were dosed orally with PS-MPs and those that

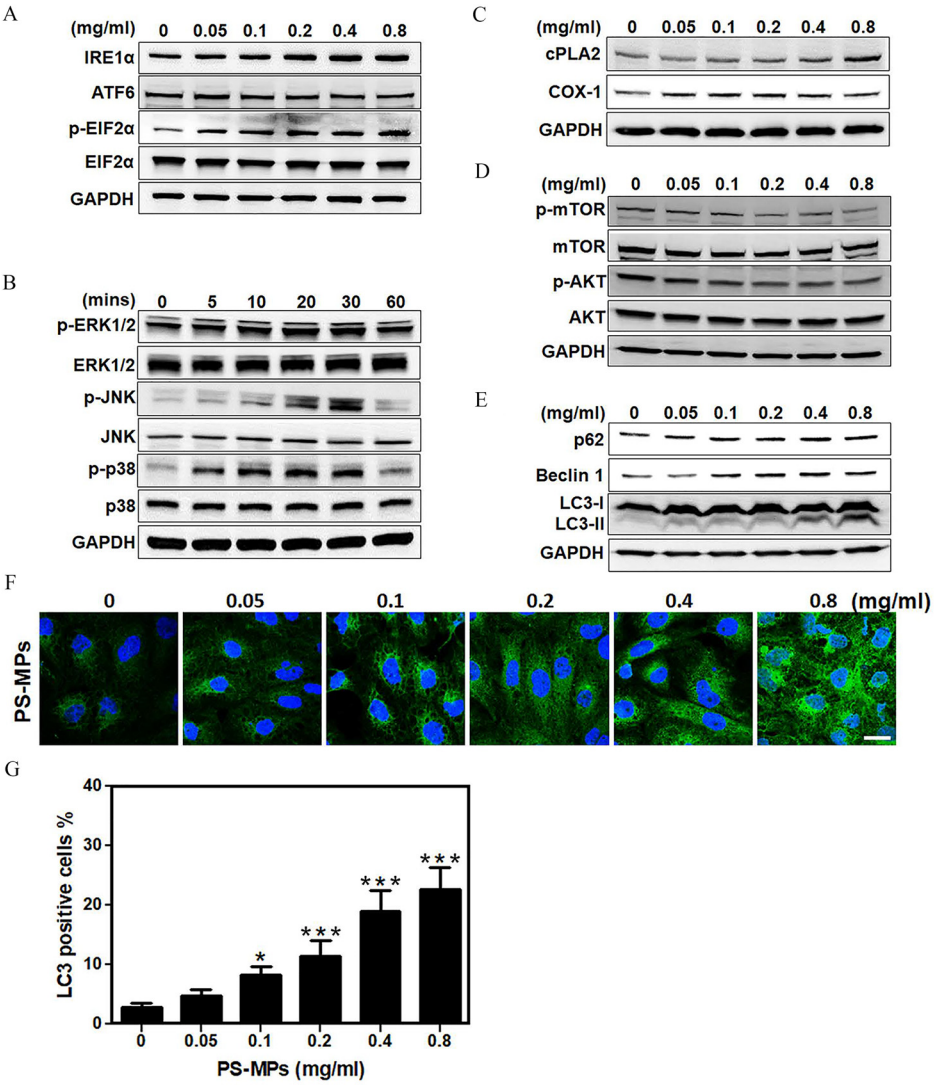

Figure 3. ER stress-related proteins, MAPK signaling pathways, inflammation-related proteins, AKT/mTOR signaling pathways, and autophagosome-related proteins in HK-2 cells treated with PS-MPs. (A) Representative western blot showing the expression of ER stress-related proteins IRE1α, ATF6, p-EIF2α, and EIF2α after PS-MPs treatment at concentrations of 0.05, 0.1, 0.2, 0.4, and 0.8 mg/mL for 24 h. (B) Representative western blot showing the expression of MAPK signaling pathway components p-ERK1/2, ERK1/2, p-JNK, JNK, p-p38, and p38 after treatment with PS-MPs at 0.8 mg/mL for 0, 5, 10, 20, 30, and 60 min. (C) Representative western blot showing the expression of inflammation-related proteins $cPLA_2$ and COX-1 after PS-MP treatment at concentrations of 0.05, 0.1, 0.2, 0.4, and 0.8 mg/mL for 24 h. (D) Representative western blot showing the expression of AKT/mTOR signaling pathway components, such as p-mTOR, mTOR, p-AKT, and AKT after treatment with PS-MPs at concentrations of 0.05, 0.1, 0.2, 0.4, and 0.8 mg/mL for 1 h. (E) Representative western blot showing the expression of autophagy-related proteins p62, Beclin 1, and LC3, after PS-MP treatment at concentrations of 0.05, 0.1, 0.2, 0.4, and 0.8 mg/mL for 24 h. GAPDH served as an internal control. (F) LC3 expression (green) was detected after treatment with PS-MPs at concentrations of 0.05, 0.1, 0.2, 0.4, and 0.8 mg/mL for 24 h in immunostaining. DAPI (blue) was used for nuclear staining. Scale bar: 25 μm. (G) The results for LC3-positive cells were graphed and statistically analyzed. $n = 3$. $^{*}p < 0.05$ and $^{***}p < 0.001$ compared with the control group, as determined by one-way ANOVA, with Dunnett's multiple comparison test. Significance: 0-mg/mL group vs. 0.1-mg/mL group: $p = 0.0265$, 0-mg/mL group vs. 0.2-mg/mL group: $p < 0.001$, 0-mg/mL group vs. 0.4-mg/mL group: $p < 0.001$, 0-mg/mL group vs. 0.8-mg/mL group: $p < 0.0015$. The data are presented as the means ± SDs. The western blotting results were quantified and statistically analyzed, as shown in Figures S3–S7. The mean and SD summary data for quantification of western blots are shown in Table S3. Note: AKT, protein kinase B; ANOVA, analysis of variance; ATF6, activating transcription factor 6; COX-1, cyclooxygenase-1; $cPLA_2$, cytoplasmic phospholipase A2; DAPI, 4,6-dimidyl-2-phenylindole; EIF2α, eukaryotic initiation factor 2 alpha; ERK1/2, extracellular signal-regulated kinases 1 and 2; GAPDH, glyceraldehyde 3-phosphate dehydrogenase; HK-2 cells, human kidney 2 cells; IRE1α, inositol-requiring enzyme 1α; JNK, c-Jun N-terminal kinase; MAPK, mitogen-activated protein kinase; mTOR, mitogen-activated protein kinase; p, phosphorylated; p-p38, phosphorylated-p38 mitogen-activated protein kinases; PS-MPs, polystyrene microplastics; SD, standard deviation.

received vehicle over the course of 4 or 8 wk of treatment (Tables S3 and S4). In addition, serum BUN did not have significant differences. However, after 4 wk of treatment, serum creatinine levels were significantly lower in the 0.2-mg/d group (0.19 ± 0.01 mg/dL) and the 0.4-mg/mL group (0.20 ± 0.01 mg/dL) than in the sham group (0.24 ± 0.02 mg/dL) (sham group vs. 0.2-mg/d group: $p = 0.001$; sham group vs. 0.4-mg/mL group: $p = 0.0026$). After 8 wk of treatment, the serum creatinine levels were lower in the 0.2-mg/d group (0.42 ± 0.01 mg/dL) and the 0.4-mg/mL group (0.38 ± 0.02 mg/dL) than in the sham group (0.45 ± 0.01 mg/dL) (sham group vs. 0.2-mg/d group: $p = 0.0068$; sham group vs. 0.4-mg/mL group: $p < 0.001$; 0.2-mg/d group vs. 0.4-mg/mL group: $p = 0.0026$) (Figure 6B). Serum creatinine is a common measure of renal function in the clinic (Lacour 1992). However, serum creatinine is also affected by muscle mass (Baxmann et al. 2008; Thongprayoon et al. 2016). As a result, we examined muscular tissue.

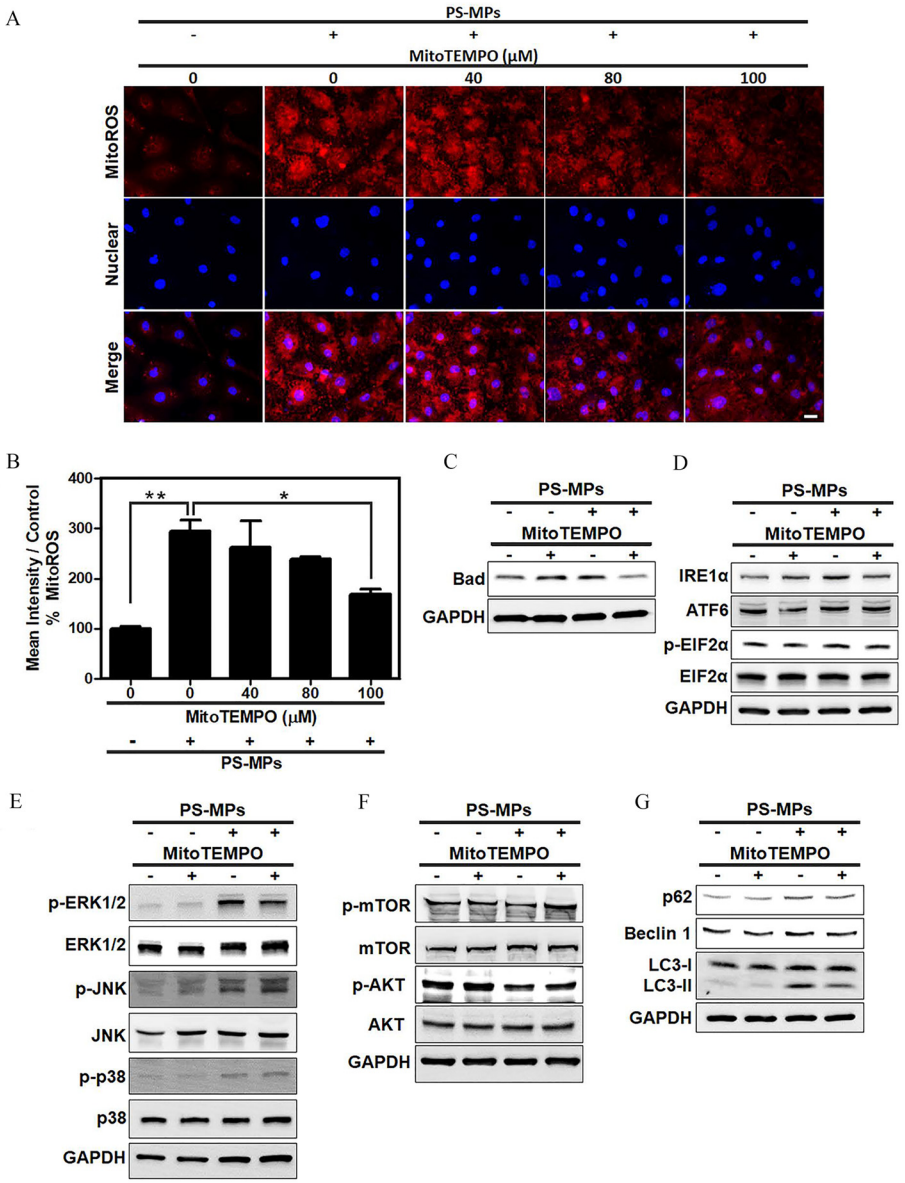

Figure 4. Levels of Bad, ER stress-related proteins, MAPK-, and AKT/mTOR signaling pathway proteins and autophagy-related proteins after PS-MP treatment in HK-2 cells with mitochondrial ROS inhibition. (A) Mitochondrial ROS levels (red) using MitoSOX Red stain after pretreatment with MitoTEMPO at concentrations of 40, 80, and 100 μM. After MitoTEMPO pretreatment, PS-MPs were added at a concentration of 0.8 mg/mL. DAPI (blue) was used for nuclear staining. Scale bar: 20 μm. (B) The mean intensity after inhibition of mitochondrial ROS production was normalized to that in the control group and graphed. $n = 3$. $^{*}p < 0.05$ and $^{**}p < 0.01$ compared with the control group, as determined by one-way ANOVA with Dunnett's multiple comparison test. Significance: 0.8-mg/mL PS-MPs group vs. 0 PS-MPs mg/mL group: $p = 0.0019$, 0.8-mg/mL PS-MP–only group vs. 0.8-mg/mL PS-MPs+100 μM MitoTEMPO group: $p = 0.0135$. The mean and SD summary data of (B) are shown in Table S3. See Table S4 for p-values for all comparisons. (C) The expression of apoptosis-related protein Bad was examined. Cells were pretreated with MitoTEMPO (100 μM) for 1 h, PS-MPs (0.8 mg/mL) were added, and the cells were incubated for another 20 min. (D) The expression of ER stress-related proteins, such as IRE1α, ATF6, p-EIF2α, and EIF2α, was examined. Cells were pretreated with MitoTEMPO for 1 h, PS-MPs were added, and the cells were incubated for another 24 h. (E) The phosphorylation of MAPK signaling pathway components p38, ERK1/2, and JNK was examined. Cells were pretreated with MitoTEMPO for 12 h, PS-MPs were added, and the cells were incubated for another 30 min. (F) The phosphorylation of AKT/mTOR pathway components mTOR, and AKT was examined. Cells were pretreated with MitoTEMPO for 1 h, PS-MPs were added, and the cells were incubated for another 1 h. (G) The expression of autophagy-related proteins p62, Beclin 1, and LC3 was examined after pretreatment with MitoTEMPO for 1 h and treatment with 0.8 mg/mL PS-MPs for 24 h. GAPDH served as an internal control. The data are presented as the means ± SDs. The mean and SD summary data for quantification of western blots are shown in Table S3. The western blotting results were quantified and statistically analyzed, as shown in Figure S8. Note: AKT, protein kinase B; ANOVA, analysis of variance; ATF6, activating transcription factor 6; DAPI, 4,6-dimidyl-2-phenylindole; EIF2α, eukaryotic initiation factor 2 alpha; ER, endoplasmic reticulum; ERK1/2, extracellular signal-regulated kinases 1 and 2; GAPDH, glyceraldehyde 3-phosphate dehydrogenase; HK-2 cells, human kidney 2 cells; IRE1α, inositol-requiring enzyme 1α; JNK, c-Jun N-terminal kinase; MAPK, mitogen-activated protein kinase; mTOR, mitogen-activated protein kinase; p, phosphorylated; PS-MPs, polystyrene microplastics; ROS, reactive oxygen species; SD, standard deviation.

As shown in Figure S10A, Masson's trichrome staining and immunostaining of dystrophin, which is primarily expressed in skeletal muscle and other muscle tissues (Gao and McNally 2015), was lower in the treatment groups compared with the sham group. The grip strength test showed that grip strength was 13% lower in the treatment groups than in the sham group (Figure S10B). Furthermore, compared with the sham group, the groups treated with PS-MPs at different concentrations for 4 and 8 wk showed different degrees of tubular injury (Figure 6C,D). IHC showed higher expression of IRE1α in the groups treated with

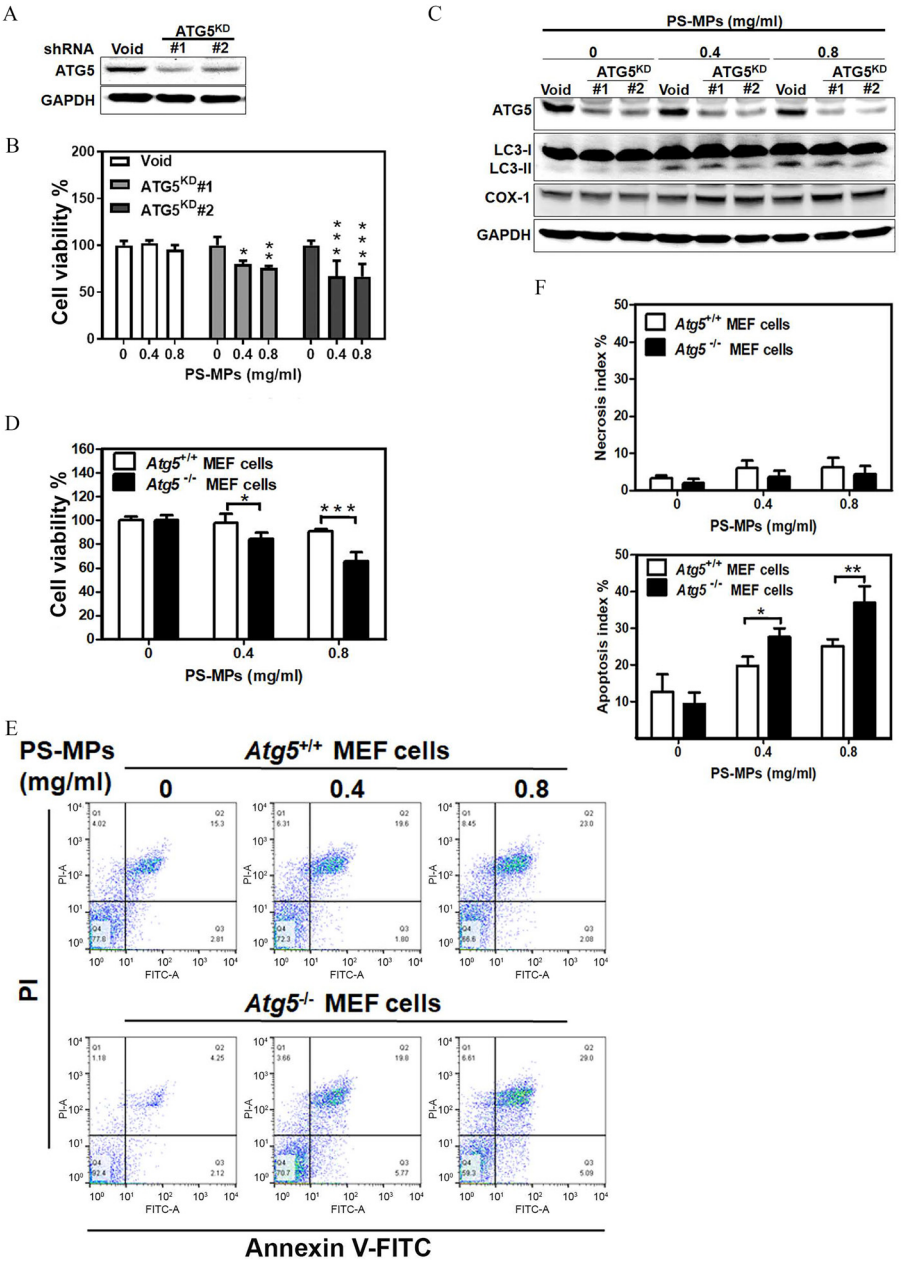

Figure 5. Cell viability and the levels of inflammation-related proteins and apoptosis in ATG5^{KD} and *Atg5*$^{-/-}$ cells treated with PS-MPs. (A) ATG5 protein expression in ATG5^{KD} and control HK-2 cells. (B) Cell viability of the ATG5^{KD} and control HK-2 cells after treatment with PS-MPs treatment at concentrations of 0.4 and 0.8 mg/mL for 48 h. $n = 3$. $^{*}p < 0.05$, $^{**}p < 0.01$, and $^{***}p < 0.001$ compared with the control group, as determined by two-way ANOVA with Dunnett's multiple comparison test. Significance: ATG5^{KD}#1: 0-mg/mL group vs. 0.4-mg/mL group: $p = 0.0174$, 0-mg/mL group vs. 0.8-mg/mL group: $p = 0.0047$; ATG5^{KD}#2: 0-mg/mL group vs. 0.4-mg/mL group: $p < 0.001$, 0-mg/mL group vs. 0.8-mg/mL group, $p < 0.001$. The mean and SD summary data of (B) are shown in Table S3. All *p*-values shown in Table S4. (C) ATG5, LC3, and COX-1 protein expression in the ATG5^{KD} and control HK-2 cells after treatment with PS-MPs at concentrations of 0.4 and 0.8 mg/mL for 48 h. (D) Cell viability of *Atg5*$^{+/+}$ and *Atg5*$^{-/-}$ MEF cells with PS-MPs at concentrations of 0.4 and 0.8 mg/mL for 48 h. $n = 3$. $^{*}p < 0.05$ and $^{***}p < 0.001$ compared with the control group, as determined by two-way ANOVA with Sidak's multiple comparisons test. Significance: *Atg5*$^{+/+}$ MEF cells vs. *Atg5*$^{-/-}$ MEF cells: 0.4-mg/mL group: $p = 0.0321$, 0.8-mg/mL group: $p < 0.001$. (E) Apoptosis of *Atg5*$^{+/+}$ and *Atg5*$^{-/-}$ MEF cells was analyzed after PS-MPs treatment at concentrations of 0.4 and 0.8 mg/mL for 48 h. The mean and SD summary data of (D) are shown in Table S3. All *p*-values shown in Table S4. (F) Necrosis and apoptosis indices in *Atg5*$^{+/+}$ and *Atg5*$^{-/-}$ MEF cells after treatment with PS-MPs at concentrations of 0.4 and 0.8 mg/mL. $n = 3$. $^{*}p < 0.05$ compared with the control group, as determined by two-way ANOVA with Sidak's multiple comparisons test. Significance: necrosis index: no significant differences (Table S3); apoptosis index: *Atg5*$^{+/+}$ MEF cells vs. *Atg5*$^{-/-}$ MEF cells: 0.4 mg/mL: $p = 0.0426$, 0.8 mg/mL: $p = 0.003$. The mean and SD summary data of (F) are shown in Table S3. All *p*-values are shown in Table S4. The data are presented as the means ± SDs. The western blotting results were quantified and statistically analyzed, as shown in Figure S9. Note: ANOVA, analysis of variance; *Atg5*$^{-/-}$, autophagy related gene 5 knockout; *Atg5*$^{+/+}$, autophagy related gene 5 wild type; ATG5^{KD}, ATG5^{KD}, autophagy related gene 5 knockdown; COX-1, cyclooxygenase-1; HK-2 cells, human kidney 2 cells; MEF, mouse embryonic fibroblast; PS-MPs, polystyrene microplastics; SD, standard deviation; shRNA, short hairpin RNA.

concentrations of 0.2 mg/d and 0.4 mg/d than in the sham group (Figure 6E). IHC staining also showed that COX-1 expression (Figure 6F) and LC3 expression (Figure 6G) were significantly higher in the PS-MP–exposed groups than in the sham group. In addition, SDS-PAGE of mouse urine was performed after oral gavage of 0.4-mg/d PS-MPs. Staining of the SDS-PAGE gel showed that the urine of the PS-MPs–treated mice had higher protein levels than that of the sham-treated mice (Figure S11A).

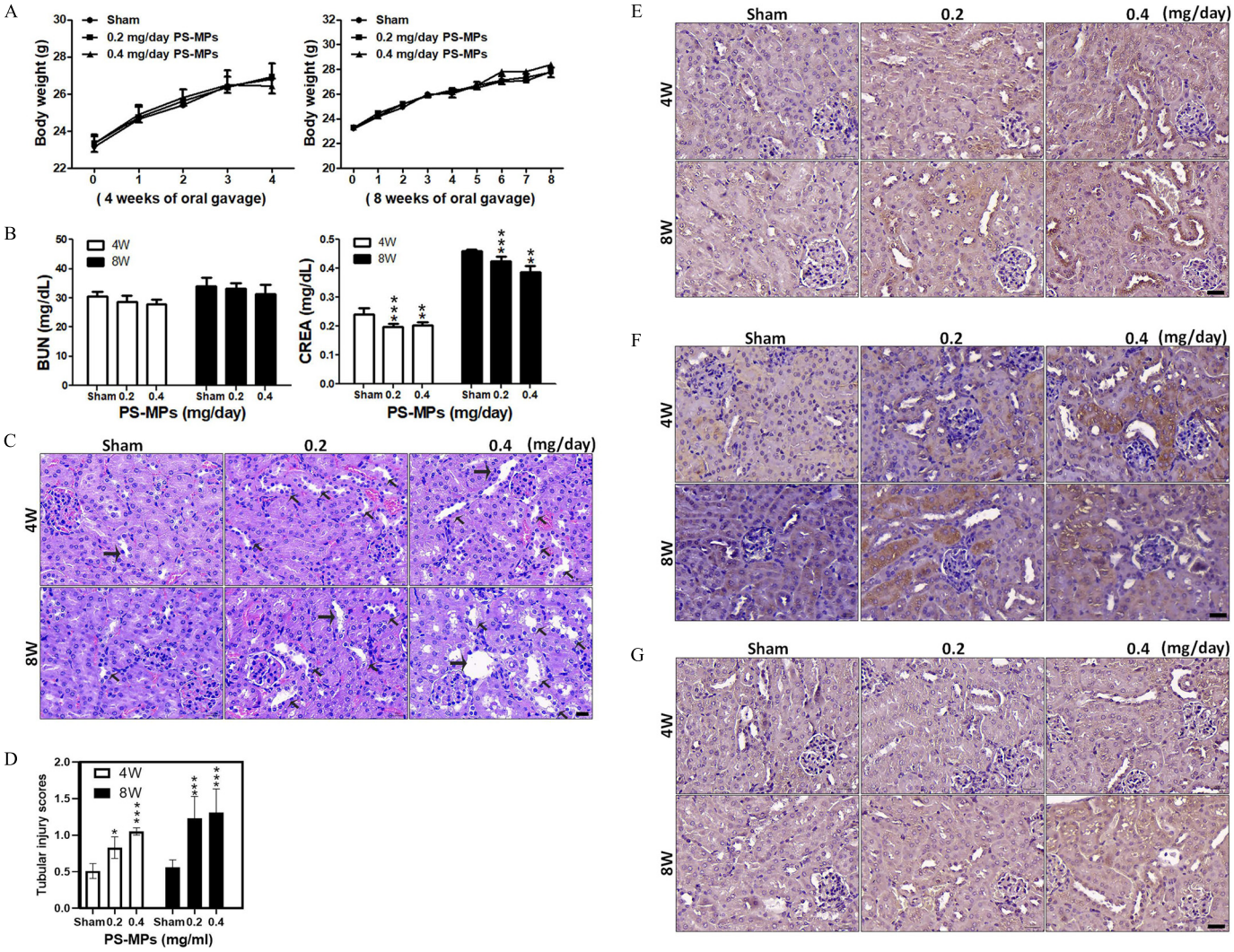

Figure 6. Body weights, blood biochemistry index values, H&E staining in kidney sections, tubulointerstitial injury, and IHC for ER stress-, inflammation-, and autophagy-related proteins in kidney sections for mice treated with PS-MPs. (A) The body weights of mice were measured after PS-MPs were administered with concentrations of 0.2 and 0.4 mg/d for 4 and 8 wk. The data are presented as the means ± SDs, $n = 5$. The mean and SD summary data of (A) are shown in Table S3. (B) Blood biochemistry was analyzed via assessment of BUN and creatinine. The data are presented as the means ± SDs. $n = 5$. $^{**}p < 0.01$ and $^{***}p < 0.001$ compared with sham group, as determined by two-way ANOVA with Tukey's multiple comparisons test. Significance: BUN: no significant differences (Table S3); creatinine: 4 wk: sham group vs. 0.2-mg/d group: $p = 0.001$, sham group vs. 0.4-mg/d group: $p = 0.0026$; 8 wk: sham group vs. 0.2-mg/d group: $p = 0.0068$, sham group vs. 0.4-mg/d group: $p < 0.05 < 0.001$, 0.2-mg/d group vs. 0.4-mg/d group: $p = 0.0026$. The mean and SD summary data of (B) are shown in Table S3. All p-values shown in Table S3. (C) H&E staining of representative kidney sections. Hematoxylin stained the cell nuclei blue, and eosin stained the extracellular matrix and cytoplasm pink. Scale bar: 30 μm. The arrows indicate lesions. (D) Tubulointerstitial injury analyses in kidneys. The data are presented as the means ± SDs. Twenty fields of view per kidney (5 mice per group). $^{*}p < 0.05$ and $^{***}p < 0.001$ compared with sham group samples, as determined by two-way ANOVA with Dunnett's multiple comparisons test. Significance: 4 wk: sham group vs. 0.2-mg/d group: $p = 0.0342$, sham group vs. 0.4-mg/d group: $p < 0.001$; and 8 wk; sham group vs. 0.2-mg/d group: $p < 0.001$, sham group vs. 0.4-mg/d group: $p < 0.001$. The mean and SD summary data of (D) are shown in Table S3. All p-values reported in Table S4. (E) IHC of IRE1α expressed in the kidney sections. Scale bar: 30 μm. (F) IHC of COX-1 expressed in the kidney sections. Scale bar: 30 μm. (G) IHC of LC3 expressed in the kidney sections. Scale bar: 30 μm. $n = 2$. The quantified IHC data were graphed and statistically analyzed, as shown in Table S5. Note: ANOVA, analysis of variance; BUN, blood urea nitrogen; COX-1, cyclooxygenase-1; CREA, creatinine; ER, endoplasmic reticulum; H&E, hematoxylin and eosin; IRE1α, inositol-requiring enzyme 1α; IHC, immunohistochemistry; PS-MPs, polystyrene microplastics; SD, standard deviation.

The urine samples showed albumin leakage (Figure S11B). We further evaluated the concentrations of PS-MPs in kidney tissues. The kidney tissues exhibited a specific Raman peak at 1,000 cm^{-1} (Wręczycki et al. 2020), giving a mean intensity of 597.4 ± 17.43, which corresponded to $3.07 \pm 0.15\ mg/g_{kidney}$ (Figure 7A–D). Statistical results of each mouse Raman analysis (Figure 7D) (sham group vs. 0.4-mg/mL group: $p < 0.001$) based on the concentration and PS-MP Raman intensity plot (Figure 7B and Table S2). Next, the ultrastructure of kidney tissues treated with PS-MPs were observed using TEM (Figure 7E). We found that PS-MPs were present in tubular epithelial cells.

Discussion

Recent studies have indicated that organs/tissues such as the gut, liver, and kidneys in mice (Deng et al. 2017b; Yang et al. 2019) and muscle tissue in northern fulmars (Herzke et al. 2016) can accumulate MPs. PS-MPs treatment can decrease mucus secretion and alter the microbiota in the gut (Lu et al. 2018) and induce inflammation in the small intestine (Li et al. 2020) in mice. However, most studies focused on liver-related variables, such as lipid accumulation (Deng et al. 2017b), changes in hepatic lipid expression (Lu et al. 2018), obvious changes in liver histopathology and alteration of serum and hepatic markers (Luo

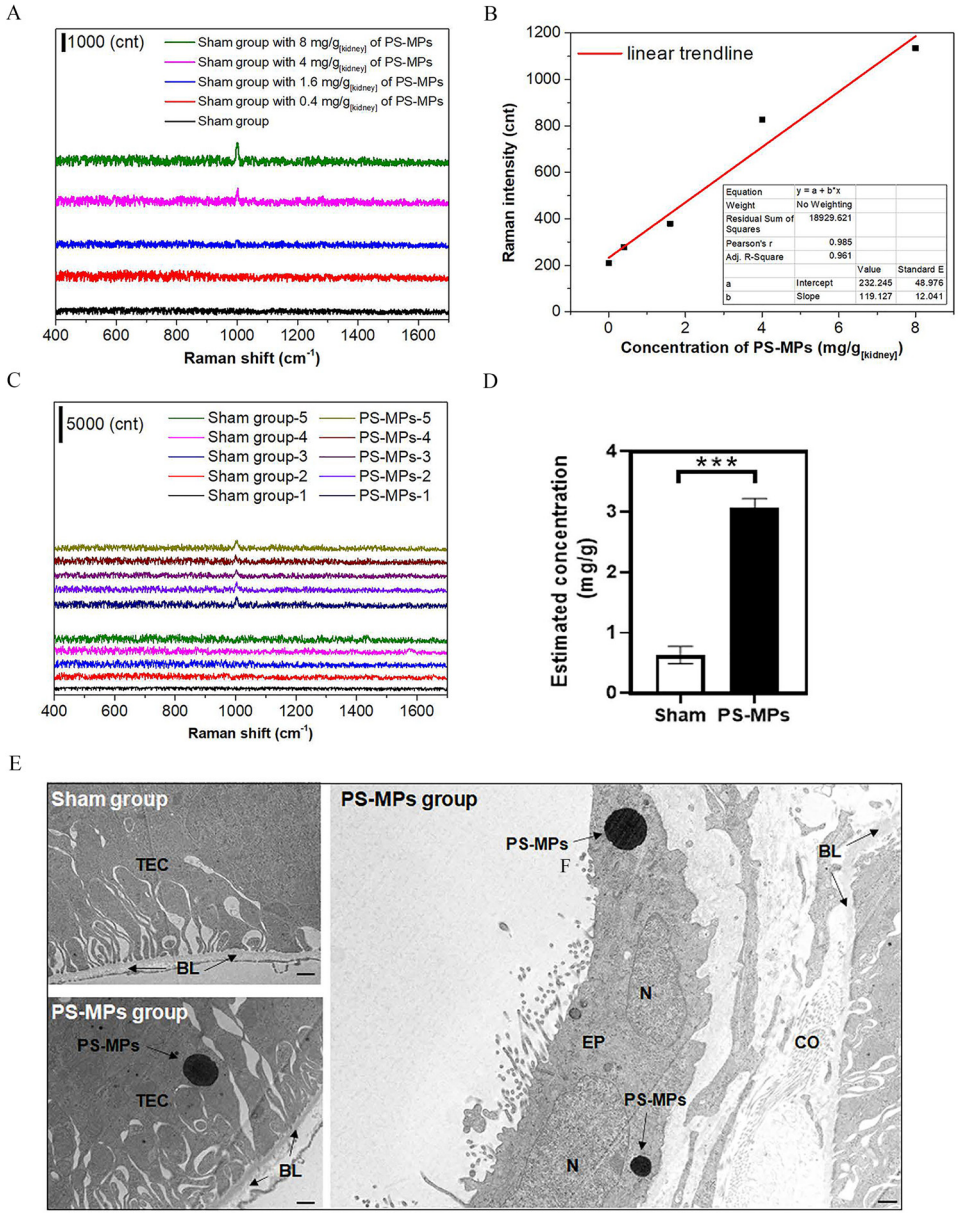

Figure 7. Raman analysis and TEM of kidney tissue from mice treated with PS-MPs. (A) Raman signals for ground kidney samples containing PS-MPs at 0, 0.4, 1.6, 4, and 8 mg/g_{kidney}. (B) Raman signal for ring breathing mode. (C) There were no Raman peaks at 1,000 cm^{-1} for the ground kidney samples of the sham-treated mice (sham group 1–5), in contrast to the samples from the mice treated with 0.4 mg/d PS-MPs for 8 wk (PS-MPs group 1–5) (Table S2). (D) Statistical results of Raman analysis for each mouse. The estimated concentrations of PS-MPs in each kidney are shown in Table S2. The mean and SD summary data of (D) are shown in Table S3. $n = 5$. $^{***}p < 0.001$ compared with the sham group, as determined by *t*-test. Significance: sham group vs. PS-MPs group: $p < 0.001$. (E) TEM analysis of the kidney tissues ($n = 3$). The sham group and PS-MPs treatment group (0.4 mg/d PS-MPs for 8 wk) were observed. Scale bar: 500 nm. Note: BL, basal lamina; cnt, count; CO, collagen fibril; EP, epithelial cell; N, nucleus; PS-MPs, polystyrene microplastics; TEC, tubular epithelial cell; SD, standard deviation; TEM, transmission electron microscopy.

et al. 2019a). Several reports have shown that PS-MPs accumulate in the kidneys in mice, but they did not determine the effects with regard to kidney damage or regulatory mechanisms (Deng et al. 2017b; Yang et al. 2019). To our knowledge, we are the first to present evidence supporting the accumulation of PS-MPs *in vitro* (in HK-2 cells) and *in vivo* (in mice). (Figures 1 and 7 and Table S2). We found that the hydrodynamic diameter of PS-MPs was 1.878 ± 0.677 μm. Notably, particles with a zeta potential >30 mV or <-30 mV have been shown to be stable in suspension and not to aggregate (Mohanraj and Chen 2006); the zeta potential of PS-MPs in the present study was -76 ± 1.2 mV, which is <-30 mV. Therefore, the particles were stable in suspension. The PDI for the PS-MPs was 0.189 (Table S1). Previous studies have demonstrated that a PDI of ~ 0.2 or below indicates that the particles are stable following dispersion (Saremi et al. 2011). We found that the PS-MPs did not affect kidney cell viability (Figure 2A). PS-MP treatment for 1 or 2 h is used for early endocytosis detection (Liu et al. 2017). However, in the present study, kidney cells treated with PS-MPs had higher levels of mitochondrial ROS, Bad, ER stress-related proteins, inflammation-related proteins, and autophagy-related proteins than found in sham-treated cells (Figures 2 and 3). A previous study showed that mitochondrial-mediated apoptosis is regulated by antiapoptotic (Bcl2) and proapoptotic (Bad and Bax) proteins (Savitskaya and Onishchenko 2015). In addition, exposure to PS-MPs in scleractinian coral regulated the JNK and ERK1/2 signaling

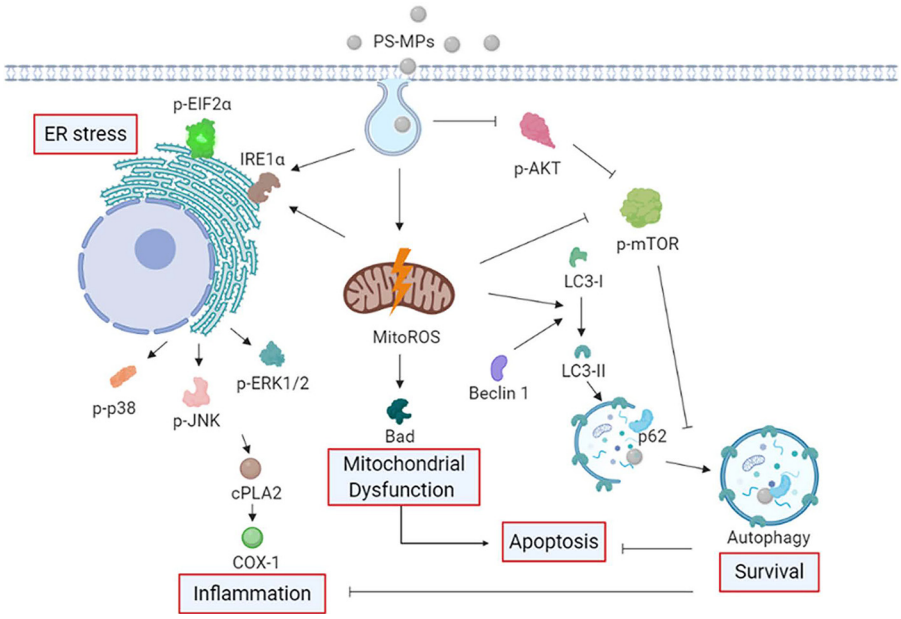

Figure 8. Schematic diagram indicating the proposed mechanism by which PS-MPs induced mitochondrial ROS production, Bad expression, ER stress, inflammation, and autophagy. Based on the data obtained in HK-2 cells and a mouse model, we propose that PS-MPs were taken up by kidney cells and that PS-MPs induced mitochondrial ROS production and Bad protein expression. Furthermore, we propose that PS-MPs increased the expression of the ER stress-related proteins IRE1α and p-EIF2α and the inflammation-related proteins $cPLA_2$ and COX-1 in kidney cells. We propose that PS-MPs increased the autophagy-related protein expression of Beclin 1, and LC3 in kidney cells and affected ER stress, inflammation, and autophagy in the kidney cells via MAPK and AKT/mTOR signaling pathways. Mitochondrial ROS-mediated regulation of Bad, IRE1α, and LC3 in kidney cells can occur via AKT/mTOR signaling pathways. Furthermore, autophagy may be an adaptive stress response that inhibits inflammation and apoptosis. Note: AKT, protein kinase B; COX-1, cyclooxygenase-1; $cPLA_2$, cytoplasmic phospholipase A2; EIF2α, eukaryotic initiation factor 2 alpha; ER, endoplasmic reticulum; HK-2 cells, human kidney 2 cells; MAPK, mitogen-activated protein kinase; mitoROS, mitochondrial reactive oxygen species; mTOR, mitogen-activated protein kinase; PS-MPs, polystyrene microplastics; ROS, reactive oxygen species.

pathways (Tang et al. 2018). We further found that protein expression in the MAPK signaling pathways (p38, JNK, and ERK1/2 signaling pathways) and AKT/mTOR signaling pathways were differentially phosphorylated (Figure 3B,D and Figure S8), suggesting that PS-MPs regulated the signaling of these pathways. Inhibition of mitochondrial ROS production mitigated the PS-MP–induced effects on Bad, IRE1α, and LC3 in HK-2 cells, suggesting that these effects occurred via the ERK1/2 and AKT/mTOR signaling pathways (Figure 4 and Figure S8). In addition, kidney tissue sections showed higher expression of IRE1α, COX-1, and LC3, similar to the findings in cells (Figure 6 and Table S5). The results showed that PS-MPs injured the kidneys.

The mechanisms of MPs cytotoxicity involve stimulation of oxidative stress via free radical generation originating from ROS (Barboza et al. 2018; Brandts et al. 2018; Liu et al. 2019; Pitt et al. 2018; Qu et al. 2018; Tang et al. 2018). ROS overproduction can alter the homeostasis of cellular components, including DNA, RNA, carbohydrates, lipids, and proteins, via consumption of antioxidant systems components. These damages were associated with physiological alterations, gene instability, and carcinogenesis (Birben et al. 2012; Nita and Grzybowski 2016). In the present study, our results indicate that PS-MPs induced oxidative stress via mitochondrial ROS (Figure 2D,E). Thus, mitochondrial ROS may play an important role in the effects of PS-MPs.

In addition, muscle tissue was shown to accumulate MPs in animals, but no related effects with regard to muscle damage or regulatory mechanisms were found (Abbasi et al. 2018; Herzke et al. 2016). As shown in Figure 6B, creatinine levels were significantly lower in mice treated with PS-MP for 4 and 8 wk. Previous studies have demonstrated that serum creatinine is affected by muscle mass (Baxmann et al. 2008; Thongprayoon et al. 2016). As shown in Figure S10A, Masson's trichrome staining and immunostaining of dystrophin showed that muscle mass was lower in the PS-MP–treated mice compared with the sham group. The grip strength test also that PS-MP–treated mice exhibited 13% lower grip strength than sham-treated mice (Figure S10B). These results suggest that the loss of muscle function occurred after PS-MP treatment. PS-MP–induced muscle dysfunction may interfere with creatinine production to result in lower kidney serum index values given that we could not find any indications of kidney injury from analysis of serum indexes, such as creatinine and BUN. In addition, we found that the urinary protein level was higher for mice treated by oral gavage with PS-MPs. The SDS-PAGE results showed that the urine of PS-MP-treated mice had higher proteins than those of sham-treated mice (Figure S11). Immunoblotting showed that one of the leaked proteins was albumin, and one sample showed higher levels than those observed in the sham group of mice (Figure S11). Some studies have shown that urinary proteins are early biomarkers of CKD (Chacar et al. 2017; Ferlizza et al. 2017; Maeda et al. 2015). The results of the present study suggest that PS-MPs not only injure the kidneys but also harm the muscle tissue.

Several studies have indicated the effects of fine particulate matter [PM ≤2.5 μm in aerodynamic diameter ($PM_{2.5}$)] on the human respiratory system (Xing et al. 2016), lung cancer, and chronic airway inflammatory diseases (Li et al. 2018). In addition, one study indicated that PM air pollution is a risk factor for CKD and end-stage renal disease (Bowe et al. 2018). We wondered whether treatment with 2-μm PS-MPs have similar effects. $PM_{2.5}$ is known to induce autophagy *in vitro* (Deng et al. 2017a; Fu et al. 2017; Zhou et al. 2017). Our results suggest that PS-MPs also induce autophagy (Figure 3E–G). We constructed stable $ATG5^{KD}$ kidney cells to prove the role of autophagy in the kidney cells (Figure 5A). We found that cell viability was lower after PS-MPs

were added to stable $ATG5^{KD}$ kidney cells compared with those treated with water (Figure 5A–C). In addition to autophagy, $PM_{2.5}$ induces apoptosis failure, which is a mode of cell death that represents a transition from apoptosis to necrosis in human lung epithelial cells (BEAS-2B cells) (Zhou et al. 2017). In the present study, cells treated with PS-MPs had higher levels of mitochondrial ROS, Bad, some ER stress-related proteins, some inflammation-related proteins, and some autophagy-related proteins in kidney cells (Figures 2 and 3 and Figure S2–S9). However, PS-MPs did not induce apoptosis in HK-2 cells (Figure 2B,C). Our results also indicated that MEF cells treated with PS-MPs did not affect cell viability compared to those treated with the vehicle alone. In contrast, in $Atg5^{-/-}$ MEFs, in which the autophagic function was knocked out, treatment with PS-MPs resulted in higher markers of apoptosis (Figure 5D–F). Autophagy sometimes acts as an adaptive stress response in kidney injury that removes protein aggregates and promotes cell survival (Riediger et al. 2011) and sometimes causes cell death by enhancing apoptosis (Chien et al. 2007). We found that inhibition of autophagy regulation can result in the expression of higher inflammation protein and cell death (Figure 5). Therefore, our results suggest that autophagy plays a protective role against PS-MP–induced kidney damage.

The World Wildlife Fund has reported that the average human ingests $\sim$5,000 mg of plastic per week (de Wit and Bigaud 2019). The average body weight of humans worldwide is 62 kg (Walpole et al. 2012). Thus, humans might be exposed to plastics at a dose of 80.64 mg/kg per week. In particular, the people who consume large amounts of sugar and seafood might ingest many MPs, according to a table of human MP consumption (Cox et al. 2019). We gavaged PS-MPs that were diluted in distilled water into the esophagus to achieve doses of 0.2 mg/d and 0.4 mg/d twice per week and continued treatment for 4 and 8 wk. According to this regimen, the maximum dose of PS-MPs in a 30-g mouse was 26.67 mg/kg per week, and this concentration altered some ER stress, inflammation, autophagy-related proteins and induced kidney abnormalities. Thus far, MPs have been found in the human stool (Schwabl et al. 2019), and MPs or NPs have been detected in many organs of different animal species (Wang et al. 2020). Current findings indicate a possible risk of long-term MP or NP accumulation in humans due to food chain contamination (Wang et al. 2020). In addition, CKD is largely attributable to common risk factors, such as hypertension and diabetes (Global Burden of Disease Study 2013 Collaborators 2015). Previous study results have shown that CKDu occurs in many countries regardless of income (Gifford et al. 2017; Jha et al. 2013). Therefore, we wonder whether long-term exposure to PS-MPs that might be a risk factor in CKDu.

Thus far, plastic control and cleanup plans have been created by many countries worldwide (Xanthos and Walker 2017). A Netherlands-based organization, the Ocean Cleanup, uses massive nets to clean the garbage that floats on the world ocean (Williams 2019). The Australian government uses filters on large drains that stop garbage from entering the ocean (Inhabitat 2018). Plastic packaging and single-use plastic items such as medical masks, plastic spoons, plastic cups, plastic drinking straws, plastic jars, plastic bags, and plastic bottles account for a large proportion of plastic waste (Claudia 2018). Many countries including the European Union, China, the USA, and the UK, have recently implemented policies to restrict single-use plastic items (Krishnan 2019). In addition, facial cleansers containing plastic particles (Duis and Coors 2016) have been banned in 15 countries (Plastic Soup Foundation 2020). Preventing MPs or NPs from synthetic fiber textiles from flowing into rivers (Carney Almroth et al. 2018) and preventing MPs from wastewater treatment plants from flowing into the oceans are important pursuits (Leslie et al. 2017). Control measures and bans on MPs or NPs can reduce the return of these materials to humans via the food chain. We hope our results can help accelerate the implementation of global bans on single-use plastics. Because of the coronavirus disease 2019 (COVID-19) outbreak, large amounts of personal protective equipment and many relatively single-use plastic products are rapidly entering our natural environment (Haque et al. 2021).

Figure 8 shows the schematic diagram of the proposed mechanism by PS-MPs in kidney cells. We have demonstrated that PS-MPs are taken up by kidney cells in mice and that PS-MPs can result in higher levels of mitochondrial ROS, as well as the expression of Bad, the ER stress-related protein IRE1α, the inflammation-related proteins $cPLA_2$ and COX-1, and the autophagy-related proteins Beclin1 and LC3. PS-MPs also can alter the phosphorylation of proteins involved in the MAPK and AKT/mTOR signaling pathways. Furthermore, inhibition of mitochondrial ROS mitigated the effects of PS-MPs on Bad, IRE1α, and LC3 levels via AKT/mTOR signaling pathways. Autophagy may be an adaptive response to PS-MP stress that alters the levels of inflammation-related proteins, such as COX-1 and apoptosis. Oral gavage of 0.2-mg/mL or 0.4-mg/mL PS-MPs in mice also affected tubular lesions and IRE1α, COX-1, and LC3 levels, as shown by IHC. Moreover, PS-MPs affects urinary proteins in treated mice. Finally, we found that PS-MPs results in muscle injury and altered muscle function, as determined by the expression of dystrophin and grip strength analysis. Thus, we found that PS-MPs may cause changes in mitochondrial ROS, Bad, ER stress-related proteins, inflammation-related proteins, and autophagy-related proteins in addition to causing kidney damage and protein leakage.

Acknowledgments

We acknowledge C.-M. Lee for his excellent technical support in transmission electron microscopy (HT7700; HITACHI) at the Taipei Medical University Core Facility. Experiments and data analysis were performed in part through the use of the Medical Research Core Facilities Center, Office of Research and Development at the China Medical University, Taichung, Taiwan. ATG5 WT and null MEF cells provided from Dr. Noboru Mizushima (Tokyo Medical and Dental University, Tokyo, Japan). This study was supported by the Ministry of Science and Technology, Taiwan (MOST 108-2314-B-039-061-MY3, MOST 109-2314-B-038-078-MY3, and MOST 109-2314-B-038-109) and by the China Medical University, Taichung, Taiwan (CMU109-N-01).

References

Abbasi S, Soltani N, Keshavarzi B, Moore F, Turner A, Hassanaghaei M. 2018. Microplastics in different tissues of fish and prawn from the Musa Estuary, Persian Gulf. Chemosphere 205:80–87, PMID: 29684694, https://doi.org/10.1016/j.chemosphere.2018.04.076.

Barboza LGA, Vieira LR, Branco V, Figueiredo N, Carvalho F, Carvalho C, et al. 2018. Microplastics cause neurotoxicity, oxidative damage and energy-related changes and interact with the bioaccumulation of mercury in the European seabass, *Dicentrarchus labrax* (Linnaeus, 1758). Aquat Toxicol 195:49–57, PMID: 29287173, https://doi.org/10.1016/j.aquatox.2017.12.008.

Baxmann AC, Ahmed MS, Marques NC, Menon VB, Pereira AB, Kirsztajn GM, et al. 2008. Influence of muscle mass and physical activity on serum and urinary creatinine and serum cystatin C. Clin J Am Soc Nephrol 3:348–354, PMID: 18235143, https://doi.org/10.2215/CJN.02870707.

Belibi F, Zafar I, Ravichandran K, Segvic AB, Jani A, Ljubanovic DG, et al. 2011. Hypoxia-inducible factor-1α (HIF-1α) and autophagy in polycystic kidney disease (PKD). Am J Physiol Renal Physiol 300(5):F1235–1F1243, PMID: 21270095, https://doi.org/10.1152/ajprenal.00348.2010.

Birben E, Sahiner UM, Sackesen C, Erzurum S, Kalayci O. 2012. Oxidative stress and antioxidant defense. World Allergy Organ J 5(1):9–19, PMID: 23268465, https://doi.org/10.1097/WOX.0b013e3182439613.

Bolisetty S, Traylor AM, Kim J, Joseph R, Ricart K, Landar A, et al. 2010. Heme oxygenase-1 inhibits renal tubular macroautophagy in acute kidney injury. J Am Soc Nephrol 21(10):1702–1712, PMID: 20705711, https://doi.org/10.1681/ASN.2010030238.

Bowe B, Xie Y, Li T, Yan Y, Xian H, Al-Aly Z. 2018. Particulate matter air pollution and the risk of incident CKD and progression to ESRD. J Am Soc Nephrol 29(1):218–230, PMID: 28935655, https://doi.org/10.1681/ASN.2017030253.

Brandts I, Teles M, Gonçalves AP, Barreto A, Franco-Martinez L, Tvarijonaviciute A, et al. 2018. Effects of nanoplastics on *Mytilus galloprovincialis* after individual and combined exposure with carbamazepine. Sci Total Environ 643:775–784, PMID: 29958167, https://doi.org/10.1016/j.scitotenv.2018.06.257.

Cai Y, Yang L, Hu G, Chen X, Niu F, Yuan L, et al. 2016. Regulation of morphine-induced synaptic alterations: role of oxidative stress, ER stress, and autophagy. J Cell Biol 215(2):245–258, PMID: 27810915, https://doi.org/10.1083/jcb.201605065.

Carbery M, O'Connor W, Palanisami T. 2018. Trophic transfer of microplastics and mixed contaminants in the marine food web and implications for human health. Environ Int 115:400–409, PMID: 29653694, https://doi.org/10.1016/j.envint.2018.03.007.

Carney Almroth BM, Åström L, Roslund S, Petersson H, Johansson M, Persson NK. 2018. Quantifying shedding of synthetic fibers from textiles; a source of microplastics released into the environment. Environ Sci Pollut Res Int 25(2):1191–1199, PMID: 29081044, https://doi.org/10.1007/s11356-017-0528-7.

Chacar F, Kogika M, Sanches TR, Caragelasco D, Martorelli C, Rodrigues C, et al. 2017. Urinary Tamm-Horsfall protein, albumin, vitamin D-binding protein, and retinol-binding protein as early biomarkers of chronic kidney disease in dogs. Physiol Rep 5(11):e13262, PMID: 28576851, https://doi.org/10.14814/phy2.13262.

Chen X, Karnovsky A, Sans MD, Andrews PC, Williams JA. 2010. Molecular characterization of the endoplasmic reticulum: insights from proteomic studies. Proteomics 10(22):4040–4052, PMID: 21080494, https://doi.org/10.1002/pmic.201000234.

Chien CT, Shyue SK, Lai MK. 2007. Bcl-xL augmentation potentially reduces ischemia/reperfusion induced proximal and distal tubular apoptosis and autophagy. Transplantation 84(9):1183–1190, PMID: 17998875, https://doi.org/10.1097/01.tp.0000287334.38933.e3.

Cho Y, Shim WJ, Jang M, Han GM, Hong SH. 2019. Abundance and characteristics of microplastics in market bivalves from South Korea. Environ Pollut 245:1107–1116, PMID: 30682745, https://doi.org/10.1016/j.envpol.2018.11.091.

Claudia G. 2018. *Single-Use Plastics: A Roadmap for Sustainability*. Nairobi, Kenya: United Nations Environment Programme. https://wedocs.unep.org/bitstream/handle/20.500.11822/25496/singleUsePlastic_sustainability.pdf [accessed 20 April 2021].

Cox KD, Covernton GA, Davies HL, Dower JF, Juanes F, Dudas SE. 2019. Human consumption of microplastics. Environ Sci Technol 53(12):7068–7074, PMID: 31184127, https://doi.org/10.1021/acs.est.9b01517.

Cybulsky AV. 2017. Endoplasmic reticulum stress, the unfolded protein response and autophagy in kidney diseases. Nat Rev Nephrol 13(11):681–696, PMID: 28970584, https://doi.org/10.1038/nrneph.2017.129.

de Wit W, Bigaud N. 2019. No plastic in nature: assessing plastic ingestion from nature to people. https://wwfint.awsassets.panda.org/downloads/plastic_ingestion_web_spreads.pdf [accessed 20 April 2021].

Deng X, Feng N, Zheng M, Ye X, Lin H, Yu X, et al. 2017a. $PM_{2.5}$ exposure-induced autophagy is mediated by lncRNA loc146880 which also promotes the migration and invasion of lung cancer cells. Biochim Biophys Acta Gen Subj 1861(2):112–125, PMID: 27836757, https://doi.org/10.1016/j.bbagen.2016.11.009.

Deng Y, Zhang Y, Lemos B, Ren H. 2017b. Tissue accumulation of microplastics in mice and biomarker responses suggest widespread health risks of exposure. Sci Rep 7:46687, PMID: 28436478, https://doi.org/10.1038/srep46687.

Deng Y, Zhang Y, Qiao R, Bonilla MM, Yang X, Ren H, et al. 2018. Evidence that microplastics aggravate the toxicity of organophosphorus flame retardants in mice (*Mus musculus*). J Hazard Mater 357:348–354, PMID: 29908513, https://doi.org/10.1016/j.jhazmat.2018.06.017.

Díaz-Torres ER, Ortega-Ortiz CD, Silva-Iñiguez L, Nene-Preciado A, Orozco ET. 2017. Floating marine debris in waters of the Mexican Central Pacific. Mar Pollut Bull 115(1–2):225–232, PMID: 27974156, https://doi.org/10.1016/j.marpolbul.2016.11.065.

Duis K, Coors A. 2016. Microplastics in the aquatic and terrestrial environment: sources (with a specific focus on personal care products), fate and effects. Environ Sci Eur 28(1):2, PMID: 27752437, https://doi.org/10.1186/s12302-015-0069-y.

Ferlizza E, Dondi F, Andreani G, Bucci D, Archer J, Isani G. 2017. Validation of an electrophoretic method to detect albuminuria in cats. J Feline Med Surg 19(8):860–868, PMID: 27555488, https://doi.org/10.1177/1098612X16664112.

Flaquer M, Lloberas N, Franquesa M, Torras J, Vidal A, Rosa JL, et al. 2010. The combination of sirolimus and rosiglitazone produces a renoprotective effect on diabetic kidney disease in rats. Life Sci 87(5–6):147–153, PMID: 20600147, https://doi.org/10.1016/j.lfs.2010.06.004.

Fu Q, Lyu D, Zhang L, Qin Z, Tang Q, Yin H, et al. 2017. Airborne particulate matter ($PM_{2.5}$) triggers autophagy in human corneal epithelial cell line. Environ Pollut 227:314–322, PMID: 28477555, https://doi.org/10.1016/j.envpol.2017.04.078.

Gao QQ, McNally EM. 2015. The dystrophin complex: structure, function, and implications for therapy. Compr Physiol 5(3):1223–1239, PMID: 26140716, https://doi.org/10.1002/cphy.c140048.

Geyer R, Jambeck JR, Law KL. 2017. Production, use, and fate of all plastics ever made. Sci Adv 3(7):e1700782, PMID: 28776036, https://doi.org/10.1126/sciadv.1700782.

Ghosh M, Stewart A, Tucker DE, Bonventre JV, Murphy RC, Leslie CC. 2004. Role of cytosolic phospholipase A_2 in prostaglandin E_2 production by lung fibroblasts. Am J Respir Cell Mol Biol 30(1):91–100, PMID: 12842849, https://doi.org/10.1165/rcmb.2003-0005OC.

Gifford FJ, Gifford RM, Eddleston M, Dhaun N. 2017. Endemic nephropathy around the world. Kidney Int Rep 2(2):282–292, PMID: 28367535, https://doi.org/10.1016/j.ekir.2016.11.003.

Global Burden of Disease Study 2013 Collaborators. 2015. Global, regional, and national incidence, prevalence, and years lived with disability for 301 acute and chronic diseases and injuries in 188 countries, 1990–2013: a systematic analysis for the Global Burden of Disease study 2013. Lancet 386(9995):743–800, PMID: 26063472, https://doi.org/10.1016/S0140-6736(15)60692-4.

Hahladakis JN, Velis CA, Weber R, Iacovidou E, Purnell P. 2018. An overview of chemical additives present in plastics: migration, release, fate and environmental impact during their use, disposal and recycling. J Hazard Mater 344:179–199, PMID: 29035713, https://doi.org/10.1016/j.jhazmat.2017.10.014.

Han P, Shao M, Guo L, Wang W, Song G, Yu X, et al. 2018. Niclosamide ethanolamine improves diabetes and diabetic kidney disease in mice. Am J Transl Res 10(4):1071–1084, PMID: 29736201.

Han P, Yuan C, Wang Y, Wang M, Weng W, Zhan H, et al. 2019. Niclosamide ethanolamine protects kidney in adriamycin nephropathy by regulating mitochondrial redox balance. Am J Transl Res 11(2):855–864, PMID: 30899385.

Hartleben B, Gödel M, Meyer-Schwesinger C, Liu S, Ulrich T, Köbler S, et al. 2010. Autophagy influences glomerular disease susceptibility and maintains podocyte homeostasis in aging mice. J Clin Invest 120(4):1084–1096, PMID: 20200449, https://doi.org/10.1172/JCI39492.

Haque MS, Uddin S, Sayem SM, Mohib KM. 2021. Coronavirus disease 2019 (covid-19) induced waste scenario: a short overview. J Environ Chem Eng 9:104660, PMID: 33194544, https://doi.org/10.1016/j.jece.2020.104660.

Hernandez LM, Xu EG, Larsson HCE, Tahara R, Maisuria VB, Tufenkji N. 2019. Plastic teabags release billions of microparticles and nanoparticles into tea. Environ Sci Technol 53(21):12300–12310, PMID: 31552738, https://doi.org/10.1021/acs.est.9b02540.

Herzke D, Anker-Nilssen T, Nøst TH, Götsch A, Christensen-Dalsgaard S, Langset M, et al. 2016. Negligible impact of ingested microplastics on tissue concentrations of persistent organic pollutants in northern fulmars off coastal Norway. Environ Sci Technol 50(4):1924–1933, PMID: 26694206, https://doi.org/10.1021/acs.est.5b04663.

Hwang I, Lee J, Huh JY, Park J, Lee HB, Ho YS, et al. 2012. Catalase deficiency accelerates diabetic renal injury through peroxisomal dysfunction. Diabetes 61(3):728–738, PMID: 22315314, https://doi.org/10.2337/db11-0584.

Inhabitat. 2018. Cheap drainage nets keep water pollution at bay in Australia. https://inhabitat.com/cheap-drainage-nets-keep-water-pollution-at-bay-in-australia/ [accessed 20 April 2021].

Iñiguez ME, Conesa JA, Fullana A. 2017. Microplastics in Spanish table salt. Sci Rep 7(1):8620, PMID: 28819264, https://doi.org/10.1038/s41598-017-09128-x.

Jambeck JR, Geyer R, Wilcox C, Siegler TR, Perryman M, Andrady A, et al. 2015. Marine pollution. Plastic waste inputs from land into the ocean. Science 347(6223):768–771, PMID: 25678662, https://doi.org/10.1126/science.1260352.

Jha V, Garcia-Garcia G, Iseki K, Li Z, Naicker S, Plattner B, et al. 2013. Chronic kidney disease: global dimension and perspectives. Lancet 382(9888):260–272, PMID: 23727169, https://doi.org/10.1016/S0140-6736(13)60687-X.

Jiang XS, Chen XM, Hua W, He JL, Liu T, Li XJ, et al. 2020. PINK1/Parkin mediated mitophagy ameliorates palmitic acid-induced apoptosis through reducing mitochondrial ROS production in podocytes. Biochem Biophys Res Commun 525(4):954–961, PMID: 32173525, https://doi.org/10.1016/j.bbrc.2020.02.170.

Jin Y, Lu L, Tu W, Luo T, Fu Z. 2019. Impacts of polystyrene microplastic on the gut barrier, microbiota and metabolism of mice. Sci Total Environ 649:308–317, PMID: 30176444, https://doi.org/10.1016/j.scitotenv.2018.08.353.

Joly FX, Coulis M. 2018. Comparison of cellulose vs. plastic cigarette filter decomposition under distinct disposal environments. Waste Manag 72:349–353, PMID: 29153904, https://doi.org/10.1016/j.wasman.2017.11.023.

Kane IA, Clare MA, Miramontes E, Wogelius R, Rothwell JJ, Garreau P, et al. 2020. Seafloor microplastic hotspots controlled by deep-sea circulation. Science 368(6495):1140–1145, PMID: 32354839, https://doi.org/10.1126/science.aba5899.

Karlsson TM, Vethaak AD, Almroth BC, Ariese F, van Velzen M, Hassellöv M, et al. 2017. Screening for microplastics in sediment, water, marine invertebrates and fish: method development and microplastic accumulation. Mar Pollut Bull 122(1–2):403–408, PMID: 28689849, https://doi.org/10.1016/j.marpolbul.2017.06.081.

Kimura T, Takabatake Y, Takahashi A, Kaimori JY, Matsui I, Namba T, et al. 2011. Autophagy protects the proximal tubule from degeneration and acute ischemic injury. J Am Soc Nephrol 22(5):902–913, PMID: 21493778, https://doi.org/10.1681/ASN.2010070705.

Kosuth M, Mason SA, Wattenberg EV. 2018. Anthropogenic contamination of tap water, beer, and sea salt. PLoS One 13(4):e0194970, PMID: 29641556, https://doi.org/10.1371/journal.pone.0194970.

Krishnan S. 2019. Single-use plastic ban: what is single-use plastic, which plastic items will be banned on October 2? https://www.jagranjosh.com/current-affairs/current-affairs-august-2019-what-is-singleuse-plastic-and-why-is-it-being-banned-1567074897-1 [accessed 20 April 2021].

Kuda O, Jenkins CM, Skinner JR, Moon SH, Su X, Gross RW, et al. 2011. CD36 protein is involved in store-operated calcium flux, phospholipase A2 activation, and production of prostaglandin E2. J Biol Chem 286(20):17785–17795, PMID: 21454644, https://doi.org/10.1074/jbc.M111.232975.

Kuma A, Hatano M, Matsui M, Yamamoto A, Nakaya H, Yoshimori T, et al. 2004. The role of autophagy during the early neonatal starvation period. Nature 432(7020):1032–1036, PMID: 15525940, https://doi.org/10.1038/nature03029.

Kutralam-Muniasamy G, Pérez-Guevara F, Elizalde-Martínez I, Shruti VC. 2020. Branded milks—are they immune from microplastics contamination? Sci Total Environ 714:136823, PMID: 31991276, https://doi.org/10.1016/j.scitotenv.2020.136823.

Lacour B. 1992. Creatinine and renal function. [In French.] Nephrologie 13(2):73–81, PMID: 1608500.

Lamb JB, Willis BL, Fiorenza EA, Couch CS, Howard R, Rader DN, et al. 2018. Plastic waste associated with disease on coral reefs. Science 359(6374):460–462, PMID: 29371469, https://doi.org/10.1126/science.aar3320.

Lebreton L, Slat B, Ferrari F, Sainte-Rose B, Aitken J, Marthouse R, et al. 2018. Evidence that the Great Pacific Garbage Patch is rapidly accumulating plastic. Sci Rep 8(1):4666, PMID: 29568057, https://doi.org/10.1038/s41598-018-22939-w.

Leslie HA, Brandsma SH, van Velzen MJM, Vethaak AD. 2017. Microplastics en route: field measurements in the Dutch river delta and Amsterdam canals, wastewater treatment plants, North Sea sediments and biota. Environ Int 101:133–142, PMID: 28143645, https://doi.org/10.1016/j.envint.2017.01.018.

Li B, Ding Y, Cheng X, Sheng D, Xu Z, Rong Q, et al. 2020. Polyethylene microplastics affect the distribution of gut microbiota and inflammation development in mice. Chemosphere 244:125492, PMID: 31809927, https://doi.org/10.1016/j.chemosphere.2019.125492.

Li J, Green C, Reynolds A, Shi H, Rotchell JM. 2018. Microplastics in mussels sampled from coastal waters and supermarkets in the United Kingdom. Environ Pollut 241:35–44, PMID: 29793106, https://doi.org/10.1016/j.envpol.2018.05.038.

Li R, Zhou R, Zhang J. 2018. Function of PM2.5 in the pathogenesis of lung cancer and chronic airway inflammatory diseases. Oncol Lett 15(5):7506–7514, PMID: 29725457, https://doi.org/10.3892/ol.2018.8355.

Liebezeit G, Liebezeit E. 2013. Non-pollen particulates in honey and sugar. Food Addit Contam Part A Chem Anal Control Expo Risk Assess 30(12):2136–2140, PMID: 24160778, https://doi.org/10.1080/19440049.2013.843025.

Liebezeit G, Liebezeit E. 2014. Synthetic particles as contaminants in German beers. Food Addit Contam Part A Chem Anal Control Expo Risk Assess 31(9):1574–1578, PMID: 25056358, https://doi.org/10.1080/19440049.2014.945099.

Liu M, Li Q, Liang L, Li J, Wang K, Li J, et al. 2017. Real-time visualization of clustering and intracellular transport of gold nanoparticles by correlative imaging. Nat Commun 8:15646, PMID: 28561031, https://doi.org/10.1038/ncomms15646.

Liu S, Hartleben B, Kretz O, Wiech T, Igarashi P, Mizushima N, et al. 2012. Autophagy plays a critical role in kidney tubule maintenance, aging and ischemia-reperfusion injury. Autophagy 8(5):826–837, PMID: 22617445, https://doi.org/10.4161/auto.19419.

Liu Z, Yu P, Cai M, Wu D, Zhang M, Huang Y, et al. 2019. Polystyrene nanoplastic exposure induces immobilization, reproduction, and stress defense in the freshwater cladoceran *Daphnia pulex*. Chemosphere 215:74–81, PMID: 30312919, https://doi.org/10.1016/j.chemosphere.2018.09.176.

Lu L, Wan Z, Luo T, Fu Z, Jin Y. 2018. Polystyrene microplastics induce gut microbiota dysbiosis and hepatic lipid metabolism disorder in mice. Sci Total Environ 631–632:449–458, PMID: 29529433, https://doi.org/10.1016/j.scitotenv.2018.03.051.

Lu Y, Zhang Y, Deng Y, Jiang W, Zhao Y, Geng J, et al. 2016. Uptake and accumulation of polystyrene microplastics in zebrafish (*Danio rerio*) and toxic effects in liver. Environ Sci Technol 50(7):4054–4060, PMID: 26950772, https://doi.org/10.1021/acs.est.6b00183.

Luo T, Wang C, Pan Z, Jin C, Fu Z, Jin Y. 2019a. Maternal polystyrene microplastic exposure during gestation and lactation altered metabolic homeostasis in the dams and their F1 and F2 offspring. Environ Sci Technol 53(18):10978–10992, PMID: 31448906, https://doi.org/10.1021/acs.est.9b03191.

Luo T, Zhang Y, Wang C, Wang X, Zhou J, Shen M, et al. 2019b. Maternal exposure to different sizes of polystyrene microplastics during gestation causes metabolic disorders in their offspring. Environ Pollut 255(pt 1):113122, PMID: 31520900, https://doi.org/10.1016/j.envpol.2019.113122.

Maeda H, Sogawa K, Sakaguchi K, Abe S, Sagizaka W, Mochizuki S, et al. 2015. Urinary albumin and transferrin as early diagnostic markers of chronic kidney disease. J Vet Med Sci 77(8):937–943, PMID: 25819688, https://doi.org/10.1292/jvms.14-0427.

Mizushima N. 2018. A brief history of autophagy from cell biology to physiology and disease. Nat Cell Biol 20(5):521–527, PMID: 29686264, https://doi.org/10.1038/s41556-018-0092-5.

Mohanraj VJ, Chen Y. 2006. Nanoparticles—a review. Trop J Pharm Res 5(1):561–573. https://doi.org/10.4314/tjpr.v5i1.14634, http://www.bioline.org.br/pdf?pr06007 [accessed 20 April 2021].

Monti DM, Guarnieri D, Napolitano G, Piccoli R, Netti P, Fusco S, et al. 2015. Biocompatibility, uptake and endocytosis pathways of polystyrene nanoparticles in primary human renal epithelial cells. J Biotechnol 193:3–10, PMID: 25444875, https://doi.org/10.1016/j.jbiotec.2014.11.004.

Moretti L, Cha YI, Niermann KJ, Lu B. 2007. Switch between apoptosis and autophagy: radiation-induced endoplasmic reticulum stress? Cell Cycle 6(7):793–798, PMID: 17377498, https://doi.org/10.4161/cc.6.7.4036.

Nita M, Grzybowski A. 2016. The role of the reactive oxygen species and oxidative stress in the pathomechanism of the age-related ocular diseases and other pathologies of the anterior and posterior eye segments in adults. Oxid Med Cell Longev 2016:3164734, PMID: 26881021, https://doi.org/10.1155/2016/3164734.

Papadopulos F, Spinelli M, Valente S, Foroni L, Orrico C, Alviano F, et al. 2017. Common tasks in microscopic and ultrastructural image analysis using imagej. Ultrastruct Pathol 31:401–407, PMID: 18098058, https://doi.org/10.1080/01913120701719189.

Pitt JA, Trevisan R, Massarsky A, Kozal JS, Levin ED, Di Giulio RT. 2018. Maternal transfer of nanoplastics to offspring in zebrafish (*Danio rerio*): a case study with nanopolystyrene. Sci Total Environ 643:324–334, PMID: 29940444, https://doi.org/10.1016/j.scitotenv.2018.06.186.

Pivokonsky M, Cermakova L, Novotna K, Peer P, Cajthaml T, Janda V. 2018. Occurrence of microplastics in raw and treated drinking water. Sci Total Environ 643:1644–1651, PMID: 30104017, https://doi.org/10.1016/j.scitotenv.2018.08.102.

Plastic Soup Foundation. 2020. Global Impact. https://www.beatthemicrobead.org/impact/global-impact/ [accessed 20 April 2021].

Qu M, Xu K, Li Y, Wong G, Wang D. 2018. Using *acs*-22 mutant *Caenorhabditis elegans* to detect the toxicity of nanopolystyrene particles. Sci Total Environ 643:119–126, PMID: 29936155, https://doi.org/10.1016/j.scitotenv.2018.06.173.

Rafiee M, Dargahi L, Eslami A, Beirami E, Jahangiri-Rad M, Sabour S, et al. 2018. Neurobehavioral assessment of rats exposed to pristine polystyrene nanoplastics upon oral exposure. Chemosphere 193:745–753, PMID: 29175402, https://doi.org/10.1016/j.chemosphere.2017.11.076.

Remy F, Collard F, Gilbert B, Compère P, Eppe G, Lepoint G. 2015. When microplastic is not plastic: the ingestion of artificial cellulose fibers by macrofauna living in seagrass macrophytodetritus. Environ Sci Technol 49(18):11158–11166, PMID: 26301775, https://doi.org/10.1021/acs.est.5b02005.

Rhodes CJ. 2018. Plastic pollution and potential solutions. Sci Prog 101(3):207–260, PMID: 30025551, https://doi.org/10.3184/003685018X15294876706211.

Riediger F, Quack I, Qadri F, Hartleben B, Park JK, Potthoff SA, et al. 2011. Prorenin receptor is essential for podocyte autophagy and survival. J Am Soc Nephrol 22(12):2193–2202, PMID: 22034640, https://doi.org/10.1681/ASN.2011020200.

Rocha M, Apostolova N, Díaz-Rua R, Muntane J, Victor VM. 2020. Mitochondria and T2D: role of autophagy, ER stress, and inflammasome. Trends Endocrinol Metab 31(10):725–741, PMID: 32265079, https://doi.org/10.1016/j.tem.2020.03.004.

Rochman CM, Browne MA, Halpern BS, Hentschel BT, Hoh E, Karapanagioti HK, et al. 2013. Policy: classify plastic waste as hazardous. Nature 494(7436):169–171, PMID: 23407523, https://doi.org/10.1038/494169a.

Saito A, Imaizumi K. 2018. Unfolded protein response-dependent communication and contact among endoplasmic reticulum, mitochondria, and plasma membrane. Int J Mol Sci 19(10):3215, PMID: 30340324, https://doi.org/10.3390/ijms19103215.

Saremi S, Atyabi F, Akhlaghi SP, Ostad SN, Dinarvand R. 2011. Thiolated chitosan nanoparticles for enhancing oral absorption of docetaxel: preparation, in vitro and ex vivo evaluation. Int J Nanomedicine 6:119–128, PMID: 21289989, https://doi.org/10.2147/IJN.S15500.

Saunders MR, Kim SD, Patel N, Meltzer DO, Chin MH. 2015. Hospitalized patients frequently unaware of their chronic kidney disease. J Hosp Med 10(9):619–622, PMID: 26014973, https://doi.org/10.1002/jhm.2395.

Savitskaya MA, Onishchenko GE. 2015. Mechanisms of apoptosis. Biochemistry (Mosc) 80(11):1393–1405, PMID: 26615431, https://doi.org/10.1134/S0006297915110012.

Schmitz KJ, Ademi C, Bertram S, Schmid KW, Baba HA. 2016. Prognostic relevance of autophagy-related markers LC3, p62/sequestosome 1, Beclin-1 and ULK1 in colorectal cancer patients with respect to KRAS mutational status. World J Surg Oncol 14(1):189, PMID: 27444698, https://doi.org/10.1186/s12957-016-0946-x.

Schwabl P, Köppel S, Königshofer P, Bucsics T, Trauner M, Reiberger T, et al. 2019. Detection of various microplastics in human stool: a prospective case series. Ann Intern Med 171(7):453–457, PMID: 31476765, https://doi.org/10.7326/M19-0618.

Schymanski D, Goldbeck C, Humpf HU, Fürst P. 2018. Analysis of microplastics in water by micro-Raman spectroscopy: release of plastic particles from different packaging into mineral water. Water Res 129:154–162, PMID: 29145085, https://doi.org/10.1016/j.watres.2017.11.011.

Serra AL, Poster D, Kistler AD, Krauer F, Raina S, Young J, et al. 2010. Sirolimus and kidney growth in autosomal dominant polycystic kidney disease. N Engl J Med 363(9):820–829, PMID: 20581391, https://doi.org/10.1056/NEJMoa0907419.

Smith M, Love DC, Rochman CM, Neff RA. 2018. Microplastics in seafood and the implications for human health. Curr Environ Health Rep 5(3):375–386, PMID: 30116998, https://doi.org/10.1007/s40572-018-0206-z.

Song YK, Hong SH, Jang M, Han GM, Jung SW, Shim WJ. 2017. Combined effects of UV exposure duration and mechanical abrasion on microplastic fragmentation by polymer type. Environ Sci Technol 51(8):4368–4376, PMID: 28249388, https://doi.org/10.1021/acs.est.6b06155.

Stock V, Böhmert L, Lisicki E, Block R, Cara-Carmona J, Pack LK, et al. 2019. Uptake and effects of orally ingested polystyrene microplastic particles in vitro and in vivo. Arch Toxicol 93(7):1817–1833, PMID: 31139862, https://doi.org/10.1007/s00204-019-02478-7.

Takahashi A, Kimura T, Takabatake Y, Namba T, Kaimori J, Kitamura H, et al. 2012. Autophagy guards against cisplatin-induced acute kidney injury. Am J Pathol 180(2):517–525, PMID: 22265049, https://doi.org/10.1016/j.ajpath.2011.11.001.

Takeshita H, Yamamoto K, Nozato S, Inagaki T, Tsuchimochi H, Shirai M, et al. 2017. Modified forelimb grip strength test detects aging-associated physiological decline in skeletal muscle function in male mice. Sci Rep 7:42323, PMID: 28176863, https://doi.org/10.1038/srep42323.

Tang J, Ni X, Zhou Z, Wang L, Lin S. 2018. Acute microplastic exposure raises stress response and suppresses detoxification and immune capacities in the scleractinian coral *Pocillopora damicornis*. Environ Pollut 243(pt A):66–74, PMID: 30172125, https://doi.org/10.1016/j.envpol.2018.08.045.

Thongprayoon C, Cheungpasitporn W, Kashani K. 2016. Serum creatinine level, a surrogate of muscle mass, predicts mortality in critically ill patients. J Thorac Dis 8(5):E305–E311, PMID: 27162688, https://doi.org/10.21037/jtd.2016.03.62.

Van Cauwenberghe L, Janssen CR. 2014. Microplastics in bivalves cultured for human consumption. Environ Pollut 193:65–70, PMID: 25005888, https://doi.org/10.1016/j.envpol.2014.06.010.

Walpole SC, Prieto-Merino D, Edwards P, Cleland J, Stevens G, Roberts I. 2012. The weight of nations: an estimation of adult human biomass. BMC Public Health 12:439, PMID: 22709383, https://doi.org/10.1186/1471-2458-12-439.

Wang T, Fu X, Chen Q, Patra JK, Wang D, Wang Z, et al. 2019. Arachidonic acid metabolism and kidney inflammation. Int J Mol Sci 20(15):3683, PMID: 31357612, https://doi.org/10.3390/ijms20153683.

Wang YL, Lee YH, Chiu IJ, Lin YF, Chiu HW. 2020. Potent impact of plastic nanomaterials and micromaterials on the food chain and human health. Int J Mol Sci 21(5):1727, PMID: 32138322, https://doi.org/10.3390/ijms21051727.

Webster AC, Nagler EV, Morton RL, Masson P. 2017. Chronic kidney disease. Lancet 389(10075):1238–1252, PMID: 27887750, https://doi.org/10.1016/S0140-6736(16)32064-5.

Welle F, Franz R. 2018. Microplastic in bottled natural mineral water—literature review and considerations on exposure and risk assessment. Food Addit Contam Part A Chem Anal Control Expo Risk Assess 35(12):2482–2492, PMID: 30451587, https://doi.org/10.1080/19440049.2018.1543957.

Williams D. 2019. A floating device created to clean up plastic from the ocean is finally doing its job, organizers say. https://www.cnn.com/2019/10/02/tech/ocean-cleanup-catching-plastic-scn-trnd/index.html [accessed 20 April 2021].

Wręczycki J, Bieliński DM, Kozanecki M, Maczugowska P, Mlostoń G. 2020. Anionic copolymerization of styrene sulfide with elemental sulfur (S_8). Materials (Basel) 13(11):2597, PMID: 32517292, https://doi.org/10.3390/ma13112597.

Wu B, Wu X, Liu S, Wang Z, Chen L. 2019. Size-dependent effects of polystyrene microplastics on cytotoxicity and efflux pump inhibition in human Caco-2 cells. Chemosphere 221:333–341, PMID: 30641374, https://doi.org/10.1016/j.chemosphere.2019.01.056.

Xanthos D, Walker TR. 2017. International policies to reduce plastic marine pollution from single-use plastics (plastic bags and microbeads): a review. Mar Pollut Bull 118(1–2):17–26, PMID: 28238328, https://doi.org/10.1016/j.marpolbul.2017.02.048.

Xing YF, Xu YH, Shi MH, Lian YX. 2016. The impact of PM2.5 on the human respiratory system. J Thorac Dis 8(1):E69–E74, PMID: 26904255, https://doi.org/10.3978/j.issn.2072-1439.2016.01.19.

Xu J, Kitada M, Koya D. 2020. The impact of mitochondrial quality control by Sirtuins on the treatment of type 2 diabetes and diabetic kidney disease. Biochim Biophys Acta Mol Basis Dis 1866(6):165756, PMID: 32147421, https://doi.org/10.1016/j.bbadis.2020.165756.

Yang YF, Chen CY, Lu TH, Liao CM. 2019. Toxicity-based toxicokinetic/toxicodynamic assessment for bioaccumulation of polystyrene microplastics in mice. J Hazard Mater 366:703–713, PMID: 30583240, https://doi.org/10.1016/j.jhazmat.2018.12.048.

Yousif E, Haddad R. 2013. Photodegradation and photostabilization of polymers, especially polystyrene: review. Springerplus 2:398, PMID: 25674392, https://doi.org/10.1186/2193-1801-2-398.

Zhang W, Liu HT. 2002. MAPK signal pathways in the regulation of cell proliferation in mammalian cells. Cell Res 12(1):9–18, PMID: 11942415, https://doi.org/10.1038/sj.cr.7290105.

Zhou W, Yuan X, Zhang L, Su B, Tian D, Li Y. 2017. Overexpression of HO-1 assisted PM2.5-induced apoptosis failure and autophagy-related cell necrosis. Ecotoxicol Environ Saf 145:605–614, PMID: 28802142, https://doi.org/10.1016/j.ecoenv.2017.07.047.